Optimized Synthesis Characterization and Protective Activity of Quercetin and Quercetin-Chitosan Nanoformula against Cardiotoxicity that was induced in Male Wister Rats via Anticancer Agent: Doxorubicin

Asmaa. G. Soliman
Beni-Suef University
Basant Mahmoud
Beni-Suef University
Zienab E. Eldin
Beni-Suef University
Ahmed A. G. El-Shahawy (Ahmed.elshahawy@psas.bsu.edu.eg)
Beni-Suef University
Mohamed Abdel-Gabbar
Beni-Suef University

Research Article

Keywords: Quercetin, Chitosan, cardiotoxicity, nanoparticles, Doxorubicin, Anticancer Agent

Posted Date: November 30th, 2022

DOI: https://doi.org/10.21203/rs.3.rs-2311749/v1

Additional Declarations: No competing interests reported.

Version of Record: A version of this preprint was published at Cancer Nanotechnology on February 13th, 2023. See the published version at https://doi.org/10.1186/s12645-023-00158-x.

Abstract

The study’s goal was to look into the protective properties of quercetin (QU) and QU-loaded chitosan nanoparticles (QU-CHSNPs) against cardiotoxicity. The ionotropic gelation approach was adopted to form QU-CHSNPs. The characterizations were performed using advanced techniques. In vitro, the release profile of QU was studied. Cardiotoxicity was induced by doxorubicin (DOX) and protected via concurrent administration of QU and QU-CHSNPs. The heart’s preventive effects of QU and QU- CHSNPs were signified by a decline in the raised serum activities of cardiac enzymes together with the improvement of the heart's antioxidant defence system and heart histological changes. The findings substantiated QU-CHSNPs' structure with an entrapment efficiency of 92.56%. The mean of the Zeta size distribution was 150 nm, the real average particle size was 50 nm, and the zeta potential value was − 27.9 mV, exhibiting low physical stability. The percent of the free QU-cumulative release was about 70% after 12 hours, and QU-CHSNPs showed a 49% continued release with a pattern of sustained release, reaching 98% after 48 hours. And as such, QU and QU-CHSNPs restrained the induced cardiotoxicity of DOX in male Wistar rats, with the QU-CHSNPs being more efficient.

1. Background

The classes of anticancer drugs induce cardiotoxicity [1]. DOX is a potent anthracycline chemotherapeutic agent for solid and hematological tumors such as leukemia, soft-tissue sarcomas, osteosarcomas, breast cancer, and lymphomas [2]. However, its clinical application is restricted because of its toxicity effects on various tissues, covering renal and cardiac [3]. According to several studies [4], the main factors of DOX toxicity are lipid peroxidation (LPO), oxidative stress, autophagy, DNA damage, and mitochondrial injury. The essential reason for DOX-induced cardiac toxicity is the overexpression of reactive oxygen species (ROS) and mitochondrial dysfunction [6]. Since cardiomyocytes have relatively low levels of antioxidant enzymes [5], they are more vulnerable to free radical mediated damage induced by DOX.

Polyphenolic compounds have both curative and preventive properties for many diseases, including heart disease, cancer, diabetes, and hypertension [7]. QU is a polyphenolic agent (flavonoid class), and is enriched in onions, plums, peppers, mangos, and berries [8]. It has anti-inflammatory, anti-cancer, anti-viral, and anti-allergic activity [9]. Additionally, QU greedily scavenges superoxide anion, lipid proxy radicals, and singlet oxygen. Further, it inhibits the activation of extracellular signal-regulated kinase and mitogen-activated protein kinase in ROS-mediated cardiomyopathy [10]. Also, QU was a robust agent versus cardiac ischemia-reperfusion injury, diabetic cardiomyopathy, and cardiotoxicity, indicating cardioprotective effects [11]. The cardioprotective effects of QU are linked to a variety of signalling pathways in the heart, including oxidative stress reduction, apoptosis inhibition, and inflammatory proteins regulation. However, the clinical treatment of QU is insufficient owing to its hydrophobic nature, low solubility, bioavailability, permeability, and the short period of metabolism without entering into the circulation [12].

In pharmaceutical management, CHSNPs are widely accepted as carriers for hydrophobic drugs to advance their therapeutic potency and diminish their toxic effects; the reason is their biocompatibility, bioactivity, biodegradability, and polycationicity [13]. Further, the CHSNPs exhibit drug targeting delivery; solubilize various hydrophobic drugs; increase bioavailability and blood circulation; enhance encapsulation efficiency; and sustain drug release [14]. In the present research, to overcome the limitations of QU, it was encapsulated in CHSNPs. The current study compared the protective effects of free QU and QU-CHSNPs against DOX-induced cardiotoxicity in Male Wister rats.

2. Materials And Methods

2.1. Materials

Extra pure QU, CHS medium-molecular weight MW (75 kDa), TPP, acetic acid, Dimethyl sulfoxide (DMSO), and ethanol were purchased from Sigma (Sigma-Aldrich Co., St. Louis, Missouri, USA). QU was suspended in a 0.9% NaCl saline solution. Hikma is an Egyptian pharmaceutical company based in Bader City, Cairo, which manufactures the DOX hydrochloride (50mg/25ml injection vial). All used chemicals and solvents were of analytical grade and high purity. Experiments were carried out with deionized water.

2.2. Synthesis of chitosan nanoparticles:

Agreeing to the ionic gelation of chitosan with TPP anions [15], the CHSNPs were formed. In brief, a solution incorporating 50 ml of 1% acetic acid, 500 mg of 85% deacetylated chitosan, and 1 mg of TPP per mL was stirred at 1400 rpm for 30 minutes to form CHSNPs. The collected pellet was adopted for characterization.

2.3. Chitosan Nanoparticles loaded with Quercetin

The procedures followed the Xu method with modification [16]. Under steady stirring for 60 minutes, 1 ml of a dissolved 0.5 g QU in ethanol was added dropwise to the CHS solution, which contained 1 g of CHS dissolved in 50 ml of glacial acetic acid (1%). Next, at a rate of 1 mL/min, a solution of 0.2 g of sodium TPP in 20 mL of deionized water was added with further stirring for 60 min. Later, the entire mixture was centrifuged at 15,000 rpm for 30 minutes. A formula of loaded, cross-linked QU-CHSNPs was obtained, washed, and dried to be characterized.

2.4. Characterizations Techniques

The XRD system was employed to characterize the crystallinity of the prepared items. Scherrer's equation determined the crystallite size:

$$D = 0.94\lambda/\beta \cos\theta \quad \text{(Eq. 1)}$$

Where D is the crystallite size, λ is the wavelength, β is the corrected full width at half the maximum of the diffraction peak, and θ is the Bragg's diffraction angle. The Fourier Transformation infrared (FTIR)

spectra of QU nano, CHS, CHSNPs, and QU-CHSNPs were reported in the transmission mode to determine the functional groups.

The surface morphology and the particle size of the prepared CHSNPs and QU-CHSNPs were investigated by a High-resolution Transmission Electron Microscope (HR-TEM) and a field emission scanning electron microscope. The Particle size distribution of the dispersed QU and QU- QU-CHSNPs were measured by Dynamic Light Scattering (DLS) method using the Stokes Einstein equation:

$D_0=k_BT/6\pi\ \eta R_H$ *(Eq. 2).*

Where D_0 is the diffusion coefficient, *kB* is the Boltzmann constant, T is the absolute temperature, and η is the viscosity of the solvent water dispersant with a refractive index of 1.330 [17]. The change in the surface charge (Zeta potential) reflecting the colloidal stability was determined by electrophoretic laser Doppler velocimetry.

2.5. In vitro Quercetin *entrapment efficiency* and release Study

The entrapment efficiency and the release percentage of QU were calculated using the *UV-Vis* spectrometer at the absorption peak of QU, (λmax) at 370–415 nm. A modified dialysis bag method was used to assess the release of QU from QU-CHSNPs [18-19]. The entrapment efficiency of QU on CHSNPs was calculated as follows: EE% = Total amount of QU-free amount of QU/Total amount of QU x 100 (Eq. 3) [20]. The concentration of the released QU was calculated as a percentage of the initial amount of the incorporated QU. All measurements were performed in triplicate.

2.6. *In vivo study*

2.6.1. Experimental animals

In this study, male Wistar rats weighing 140–160 g served as the experimental animals. They were purchased from the Pharmacy Faculty's Animal House at Nahda University in Beni-Suef, Egypt. They were kept under tight care and monitoring for 14 days prior to the beginning of the study to rule out any concurrent infections. Animals were kept in cages with six rats per cage throughout the experiment. The selected animals were kept in typical polypropylene cages and maintained under normal atmospheric room temperature (22 ± 2◦C), humidity (55 ± 5%), illumination (12 h light/12 h dark cycles). At all times, water and a typical, balanced diet were made available to the rats. All animal procedures have been approved by the experimental animal ethics committee of the Faculty of Science at Beni-Suef University in Egypt and are in compliance with the guidelines for the humane care and use of laboratory animals published by the Canadian Council on Animal Care (CCAC) in 1993. (BSU/FS/2019/2 is the ethics approval number.) Every effort was made to lessen the number of animals used and their suffering.

2.6.2. Experimental design

In the current study, 30 rats were used. These rats were divided into five (n = 6) groups as follows: Group 1 (Normal control): Normal healthy rats were given an equivalent volume of 0.9% NaCl (2ml/kg, three days/week) by oral gavage for six weeks. Group 2 (Doxorubicin–administered control): The rats were given doxorubicin intraperitoneally at a dose of 1.25 mg/kg/48 h for six consecutive doses over two weeks to induce cardiotoxicity (I.P. injection). Group 3 (DOX-administered group treated with QU): On the same day that DOX administration began, QU (10 mg/kg, three times per week, orally) began as well. After DOX was stopped, QU was administered concurrently for an additional four weeks (a six-week total period). Group 4 (DOX-administered group treated with QU-CHSNPs): On the same day that DOX began, QU-CHSNPs (10 mg/kg, three times per week) began and continued for an additional four weeks after DOX was stopped (a six-week total period). Group 5 (normal group): Normal healthy rats were orally treated with QU-CHSNPs (10 mg/kg b. wt/day) by oral gavage for 6 weeks [21, 22].

2.6.3. Serum and tissue sampling

At the end of the six-week period, six rats from each group were slaughtered under mild diethyl ether anesthesia. Jugular vein blood was drawn from each rat and placed in a centrifuge tube, where it was allowed to coagulate for 45 minutes at room temperature. In preparation for a biochemical analysis, interleukins, and cytokine parameters, the serum samples were separated by centrifugation at 3000 rpm for ten minutes at 30^{o}C. They were then frozen and kept at -20^{o}C. Each animal's fresh heart was quickly removed and infused with sterile normal saline. Each rat's cardiac tissue was immediately removed, weighed, and stored in RNA Latter for gene expression investigation. For a 24-hour period, portions of the heart were fixed in 10% neutral buffered formalin before being moved to 70% alcohol for histopathological analysis. To determine some oxidative stress and antioxidant parameters, portions of fresh heart samples were kept at -20 oC. 0.5g from each heart was homogenized in 5ml of 0.9% sterilized sodium chloride (10% w/v) using a Teflon homogenizer (Glass-Col, Terre Haute, USA). Each rat's heart tissue was immediately excised and fixed in 7.2 percent glutaraldehyde for examination under an electron microscope. Part of cardiac tissue from each rat was immediately removed and was stored frozen for gel electrophoresis of DNA fragmentation.

3. Biochemical Analyses:

3.1. Determination of Serum heart function

Creatine kinase-MB (CK-MB) activity in serum was measured by a kinetic method using kits developed by Spectrum Diagnostics, Egypt based on the method of [23]. Using reagent kits purchased from Bio System Company (Spain), aspartate aminotransferase (AST) activity in serum was determined by a kinetic method in accordance with the method of [24]. The kinetic method described in [25] was used to measure the lactate dehydrogenase (LDH) activity in serum using reagent kits obtained from Human (Germany). The Rat Cardiac Troponin-I ELISA Kit with Catalog Number CSB-E08594r from CUSABIO was used to measure serum cardiac troponin-I levels. The serum concentrations of rat cardiac troponin (c Tn-I) are

determined quantitatively using this assay. The quantitative sandwich enzyme immunoassay method is used in this assay.

3.2. Determination of serum lipid profile

Using a reagent kit obtained from Spinreact Co (Spain), the amount of cholesterol in the serum was measured using the method of [26]. A reagent kit purchased from Spinreact Company (Spain) was used to evaluate the serum triglyceride concentration (TG) using the method described in [26]. The method of [26] was used to assess the serum HDL-c concentration using reagent kits purchased from Spinreact Co. (Spain). The amount of LDL c in the blood was calculated using the formula given in [27]: LDL-c concentration (mg/dL) = Total cholesterol - (TG/5)-HDL-c. The concentration of VLDL-c in serum was calculated using the [28] formula: VLDL-c concentration (mg/dL) = TG /5.

3.3. Estimation of activity and concentration of antioxidant markers and oxidative stress:

The activities of myocardial superoxide dismutase (SOD), glutathione S-transferase (GST) [29], glutathione peroxidase (GPx) [30], glutathione (GSH) [31], lipid peroxidation (Malondialdehyde MDA) [32], and Nitric Oxide (NO) [33] in cardiac tissue homogenate were measured using a commercial kit (Bio Diagnostic, Egypt) and based on a previously described colorimetric method.

3.4. Measurement of serum pro-inflammatory Interleukin-1Beta (IL-1β), Tumor necrosis factor- alpha (TNF-*α*) and anti-inflammatory Interleukin-10 (IL-10):

Rat Interleukin-10 (IL-10) ELISA Kit, Cat. No. MBS764911, from My BioSource, depending on sandwich enzyme-linked immune-sorbent assay technology, was used to assess IL-10 activity. Also, rat Interleukin-1B activity was measured using the rat Interleukin-1B (IL-1B) ELISA Kit User Manual Catalog # MBS825017. CUSABIO's CSB-E11987 rat (TNF-*α*) ELISA Kit was used to measure TNF-*α* activity. The concentrations of (IL-10), TNF-*α*, and IL-1B were assayed using ELISA assay kits (Assay Pro, USA).

3.5. Measurement of serum apoptotic marker Caspase-3(Casp-3).

Using the Rat Casp-3 ELISA Kit, Cat. No. CSB-E08857r from CUSABIO, casp-3 activity in serum was determined. The quantitative sandwich enzyme immunoassay method is used in this assay.

3.6. Detection of NrF2, PPAR-γ and Annexin-V molecular gene expression by quantitative Real time Polymerase Chain Reaction (QRT-PCR):

The levels of nuclear factor erythroid 2-related factor 2 (Nrf2), peroxisome proliferator-activated receptor gamma (PPAR-γ), and Annexin-V were assessed in heart tissue using the quantitative real-time polymerase chain reaction (QRT-PCR) technique. In brief, the Qiagen tissue extraction kit (Qiagen, USA) was used to extract RNA from the heart tissue of all rats. Total RNA (0.5-2 ug) was used for cDNA transformation using a high-capacity cDNA reverse transcription kit according to the manufacturer's instructions (Fermentas, USA). The β-actin gene was used as a reference. An Applied Biosystem with

software version 3.1(Step One™, USA) was used for the QRT-PCR amplification and analysis. The QRT-PCR assay using the primer sets was calibrated to work best at the annealing temperature. SYBR Green was used to monitor the synthesis of double-stranded DNA. The amplifications were completed by using 40 cycles of denaturation at 95^{o}C for 15 and annealing and extension at 60^{o}C for one minute. The Step One Plus real-time thermal cycler (Applied Biosystems, Life Technology, USA) was used for analysis and amplification. The following primers were used. Nrf2; Forward: 5'-TTGTAGATGACCATGAGTCGC-3', Reverse: 5'- TGTCCTGCTGTATGCTGCTT-3'. Annexin -V Forward: 5'-CTC TGT TTG GCA GGG ACC TT-3' Reverse: 5'- GGC ATC GTA GAG TCG TGA GG-3'. PPAR-γ Forward: 5'-GGACGCTGAAGAAGAGACCTG-3', Reverse: 5'- CCGGGTCCTGTCTGAGTATG -3'. B-actin Forward: 5'- TAC AACCTTCTT GCA GCT CCT-3', Reverse: 5'-CCT TCT GAC CCA TAC CCA CC-3'.

3.7. DNA Fragmentation Assay by Agarose Gel Electrophoresis

Apoptosis is linked to the detection of the traditional DNA laddering in cardiac extracts. The lysis solution (1% SDS, 10 mM Tris HCl, 50 mM EDTA, pH 7.4) was used to homogenize frozen hearts (one g), using an Ultra-Turrax T25 homogenizer from Janke and Kunkel IKA-Laboratory. Samples were treated with RNAsa (1 mg/ml) from Sigma Chemical Corporation for two hours at 37°C and proteinase K (1 mg/ml) for 45 minutes at 48°C. DNA was extracted using phenol, chloroform, and isoamyl alcohol 25:24:1 (Sigma Chemical Corporation) and precipitated for 12 hours at 20°C with isopropanol (v/v) and 0.5 M NaCl. Centrifugation at 15000g for 20 minutes was used to recover the DNA, and the pellet was then washed with 70% ethanol, dried, and resuspended in Tris-EDTA buffer (10 mM Tris, 50 mM EDTA), which has a pH of 7.4. Ethidium bromide (0.5 ug/ml) was added to samples (250 g DNA) for analysis on a 2% agarose gel.

3.8. Transmission Electron Microscopy (TEM) examination of heart

The samples were fixed for two hours at room temperature in three percent glutaraldehyde in 0.1 M sodium cacodylate buffer (pH 7.0), washed in the same solution, and then post-fixed for two hours in one percent osmium tetroxide. The samples were dehydrated for 15 minutes in each ethyl alcohol dilution, ranging from 10% to 90%, and then for 30 minutes in absolute ethanol. In a graded series of tests, samples were penetrated with epoxy resin and acetone until finally in pure resin. Formvar-coated copper grids were used to collect ultrathin sections. The sections were then dyed twice with uranyl acetate, followed by lead citrate. Stained sections were examined using a JEOL JEM 1010 TEM at 70 kV at Al-Azhar University's Regional Center for Mycology and Biotechnology (RCMB) [34].

3.9. Histopathological examination of heart

The heart was removed immediately after the rats were slaughtered. It was washed with saline, fixed in ten percent neutral buffered formalin for twenty-four hours, dehydrated with serial dilutions of ethyl alcohol solutions (70%, 95%, and absolute ethanol), immersed in paraffin, sectioned with a microtome at 4-5 m thickness, and stained with hematoxylin and eosin for histopathological examination under the light electric microscope.

4. Statistical Analysis

The one-way-anova statistical analysis was used to compare the data between groups, and then the Tukey-Kramer post-hoc analysis procedure was used. The results were expressed as a mean ± standard error. For all data, the statistical significance interval is $P < 0.05$. The Statistical Package for Social/Science (SPSS) version 22 software was used on Windows 10 to evaluate all the data.

Results And Discussion

Qualitative analysis of XRD

The XRD spectra for QU nano, CHS, CHSNPs, and QU- CHSNPs are shown in Figure 1. For CHS, the XRD spectrum had a low diffraction signal intensity, which reflected its low level of crystallinity. With a d-spacing of 4.43, the highest peak at 19.9° represents a relative intensity of 100%. According to Eq 1, the calculated crystallite size of the pure CHS was 128.878 Å with a micro-strain of 1.72%. It is important to note that as the width of the peak increases, the crystallite size decreases.

The XRD spectrum of CHSNPs had a disordered arrangement of CHS chains, showing a wide diffuse hump peak at around 30^o, which is a typical fingerprint of semi-crystalline chitosan [35]. Our findings were proportionate with those of a former study [36], which showed that TPP counter-ions induce cross-linking among CHS chains, and thus the construction of an opaque network that vanishes in the diffraction peaks of CHS, which form a single floppy peak. The broad peak indicated a decrease in crystallite size, reflecting a reduction in periodicity, i.e., the long-range order of atoms, ions, or molecules in the particles, and consequently, there was low ordering of the hkl planes, which decreased crystallinity. The low degree of crystalline perfection may also be attributed to the high number of defects in the nucleation and the growth rate of the crystals as a result of using polymer like chitosan [37].

According to the chemical structure of QU, scheme 1, the previously published XRD spectrum for QU confirmed its crystallinity state [38]. In our study, the nanoscale crystallinity of QU was determined by high-resolution XRD to enhance our understanding of its chemical action. The obtained XRD spectrum of QU nano had similar peaks to [38]; they were in slightly different positions. The XRD spectrum of QU nano had peaks at 8.9^o, 9.7^o, 10.7^o, 12.4^o, 13.1^o, 13.6^o, 16.6^o, 23.1^o, 24.8^o, 26.1^o, 27.4^o, 28.1^o, 28.5^o, 38.6^o, and 41.9^o, respectively. There was a high basal diffraction peak at the diffraction angle of 13.6^o with 100% relative intensity, d-spacing of 6.77 Å, a crystallite size of 485.6 Å, and a micro-strain of 0.69%. This peak was coordinated with prior research [39]. These distinct diffraction peaks indicate that the crystallinity of QU nano did not change, in agreement with previous research [40].

The same Fig 1 paraded the crystal form of QU-CHSNPs with a trick peak shifting to the left. The position of the diffracted peak can shift in response to several different factors, including substitution doping, temperature, and stress. Here, the shifting could be because of differences in interaction angles caused by changes in the QU's arrangement structure plans during the loading process. Another explanation for peak shifting was the changes in the interatomic distances of the QU-CHSNPs, which resulted from the

entrapped QU within the CHSNPs. According to the chemical structure of CHS and QU (Scheme 1), we suggest that a chemical bonding occurred between the CHS's amino group NH_2 and the CO carbonyl and OH hydroxyl functional groups of the QU. The diffracted peak of QU disappeared, enforcing this suggestion. The shifting may also be because of the adsorption of QU on the surface of CHSNPs. Overall, the QU-CHSNPs spectrum showed languid diffracted signal changes in shape, position, and the relative integrated intensity between 2 theta angles, which is agree with Zhang et al. [41]. These alterations show that there was QU loading on the CHSNPs.

FTIR spectra analysis

In figure 2, comparing to the standard QU [38], the FTIR spectrum of QU nano presented a variation of sharp, intense, and faint peaks as well as essential practical groups that corresponded to the stretching vibrations of O-H, =C-H, -CH_2, C=O, C-O, and C=C. While the spectrum exhibited peaks similar to those previously reported, there were shifts in position and intensity. The spectrum revealed a specific strong stretching peak of the carbonyl group C=O at 1660 cm^{-1}, a weak peak referred to as the =C-H stretching vibration at 2937 cm^{-1}, and a peak that indicates C=C aromatic stretching at 1511 cm^{-1}. There was a distinct peak at 3283 cm^{-1} that coincides with the stretching vibration of hydroxyl group OH, and another at 880 cm^{-1} that corresponds to a benzene ring. The obtained results reflect the molecular structure of QU.

The FTIR spectra for CHS and CHSNPs are also presented in Fig. 2. Considering the chemical structure of CHS, the presented broad peak at 3437 cm^{-1} is attributed to the stretching vibration of the OH group. A polysaccharide peak of CHS, which is in-plane N-H bending vibration, appeared at 1637 cm^{-1}. The C-O stretching vibration of the primary alcoholic group's evidence is at 1385.34 cm^{-1}, while a bending vibration peak of C-N is presented at1076 cm^{-1}. Regarding the CHSNPs spectrum, the two spectra appeared to be similar and showed various characteristic peaks with a faint diversity in the wideness and non-considerable shifting of the peak position. The broad peak ranged from 3353.09–3172.46 cm^{-1}, which corresponded to overlapping among the stretching vibrations of the O–H and N–H groups. The peaks at 2919.18 cm^{-1} were associated with aliphatic sp3 C-H stretching, those at 1636.91 cm^{-1} with in-plane N-H bending vibrations, and those at 1405.34 cm^{-1} with C-O stretching vibrations. The peak at 1020 cm^{-1}, which appears in the FTIR spectrum for CHSNPs, shows a characteristic P=O stretching vibration from the phosphate groups of the TPP. A previous study [42] reported similar results for the formation of CHSNPs treated with TPP.

The pattern of intramolecular hydrogen bonds may explain the broadness divergence between CHS and CHSNPs. Furthermore, the observed hypochromic shifting in peak positions was due to the interactions between the NH^{3+} groups of the CHS and phosphate groups of the TPP. For this reason, the FTIR spectra were employed to verify TPP and CHSNPs. The decline in amide I band intensity for CHSNPs (1636 cm^{-1}) when compared to CHS (1637 cm^{-1}) enforced this interaction. The –CH_2 wagging peak at1405 cm^{-1} was another substantial for CHSNPs.

The spectrum of QU-CHSNPs revealed significant variations in the peak patterns, intensities, and positions. For example, the broad band extended from 3500–3000 cm^{-1} due to the intermolecular hydrogen bonding, as well as the disappearance of some peaks. These variations reflected a type of interaction between CHSNPs and QU, confirming the loading process. These results were in accordance with those of previous research [43].

Surface morphology TEM and SEM study

Employing high-resolution transmission electron microscopy (HRTEM) to study the shape and particle size, the HRTEM images of CHSNPs and QU-CHSNPs are shown in Fig 3. An optimized spherical shape of the prepared CHSNPs with an average particle size of approximately 50 nm is shown in Fig 3 (A), while an HRTEM with a low field of view revealing stack clusters of the prepared QU-CHSNPs is shown in Fig 3 (B). The images display two different signal intensities, dark and gray, which might be due to a variation in the attenuation of the incident electron beam on the QU-CHSNPs. This attenuation is based on the variations in the electron densities of the QU and CHSNPs, affirming the loading process. In the HRTEM images, the appearance of darker regions inside the particles indicates the lipophilic QU in the matrix of the CHSNPs, and gray regions may indicate soluble CHS. The surface microstructures show that the sample was coated with gold to avoid charges and promote the signals needed for surface analysis with the SEM, Fig 3. The CHSNPs had a non-homogeneous, rough, and irregular surface texture, Fig 3 (C); this irregularity could be due to the complex's formation scheme, which includes incorporating two aqueous phases, one containing polymer CHS and the other containing poly-anion TPP. In contrast, the SEM image of QU-CHSNPs had a smooth surface pattern with morphology like a pineapple, Fig 3 (D).

Zeta sizer and potential measurements

The hydrodynamic size distribution of the QU nano and QU-CHSNPs was determined by the intensity distribution method via dynamic light scattering (DLS) technique, as shown in Fig 4 (A). The intensity-distribution and cumulant fit sizes were similar, and The Z average, or called cumulant mean, or log mean of the hydrodynamic diameter size distribution of QU nano was 150 nm. The polydispersity index PDI value (.992) predicted a wide width of the distribution peak, indicating a heterogeneous size distribution. The intercept value (1.09) indicated an excellent signal-to-noise ratio. For the QU-CHSNPs the reported hydrodynamic size, PDI, and the intercept were 329.4 nm, 0.541, and 0.983, respectively (Figure 4). The hydrodynamic diameter size distribution of QU-CHSNPs was slightly bigger than that identified using the HRTEM.

However, this discrepancy is reasonable as the distribution number (from electron microscopy) is expected by smaller than the distribution intensity (from DLS). In other words, the particle size determined using the DLS represents its hydrodynamic diameter, whereas that obtained using HRTEM represents its real diameter. The surface charge of the QU-CHSNPs formula was estimated by measuring the zeta potential. In total, a zeta potential value of greater than 30 mV is thought to be a standard value that will give ample repulsion force to limit particle aggregation. The repulsion among particles indicated that the

low zeta potential value was -27.9 ± 6.8 mV, which indicates low physical stability. QU is a hydrophobic polyphenol with a pentahydroxy flavone and five hydroxy groups at the 3-, 3'-, 4'-, 5-, and 7-positions, (Scheme 1). The negative charge of the formula was due to the hydroxy group, indicating the successful entrapment of QU by cross-linked CHSNPs.

Entrapment efficiency and release profiles

The results from Eq. 3 showed that the average entrapment efficiency for the QU in CHSNPs was 92.56% ±7.72%. The release profiles for the free QU and the QU from the CHSNPs in the PBS solution at a constant temperature (37°C) and pH 6.8 for 48 h are shown in Fig 4 (B). A surge release of 47.2% was observed from free QU within the first 4 hours, whereas QU-CHSNPs showed a slaw burst release of 29.21%. Free QU was released faster than QU-CHSNPs, which could be attributed to the existence of QU in the CHS's network. The initial rapid release of the loaded QU may be due to the rapid dispersion of the QU present on the surface of the CHSNPs, while at a later stage, QU may also be constantly released from the core of the CHS matrix because of CHS hydration and swelling. The drug was therefore released more gradually, and the rate of release was influenced not by polymer erosion but by drug diffusion through the amorphous territory of the polymer matrix. The free QU cumulative release in a saturation state after 12 h was approximately 70%, while that of QU-CHSNPs was 49% and it showed a pattern of sustained release, reaching 98% after 48 h. This was explained previously [44], as CHS was found to be a biodegradable polymer. However, its biodegradation is substantially slower than that of other degradable polymers. In addition, the deterioration of CHS was particularly limited in an aqueous medium because of its poor crystallinity and hydrophobicity.

Therefore, the only possible mechanism of QU release was diffusion, and not the degradation of the CHS polymer. Furthermore, it is worth noting that the diffraction pattern of the QU-CHSNPs showed that some of the QU crystal peaks had disappeared, suggesting the amorphous pattern of QU in the matrix of CHSNPs polymer or that it was dispersed in the amorphous region of the CHSNPs. Consequently, the cumulative drug percentages of the free QU were lower than those of QU-CHSNPs, attributing to the slow diffusion of QU from the CHSNPs matrix.

Biological study

Doxorubicin (brand name: Adriamycin) is a chemotherapy drug made from *Streptomyces peucetiu*. It is used together with other chemotherapy agents against malignant neoplasms, including breast cancer, lung cancer, leukemia, Hodgkin's disease, Kaposi's sarcoma, acute lymphoblastic, leukemia, lymphomas, and several metastatic tumors. Through the intercalation, DOX merges with DNA and hinders the macromolecular biosynthesis, restricting the DNA double helix formation and blocking the DNA replication process [45]. However, the long-term use of DOX produce severe effects, which restricts its clinical applications [46]. Cardiotoxicity is one of the extremely serious effects of DOX as it can lead to dilated cardiomyopathy, which results in congestive heart failure. The DOX aggregation dose controls the cardiomyopathy rate. Oxidative stress, downregulation of genes for contractile proteins, and p53-mediated apoptosis are the avenues of cardiomyopathy promoted by DOX [47].

Oxidative stress

There is abundant evidence that oxidative stress plays an essential role in the pathophysiology of DOX-induced cardiotoxicity. In cardiomyocytes, DOX can lose one electron through the metabolic efficiency of Nicotinamide Adenine Dinucleotide/Phosphate-cytochrome P 450 reductase. The DOX reduction forms semiquinone free radicals, which produce radicals of hydroxyl (•OH), hydrogen peroxide (H_2O_2), and proxynitrite (ONOO) [48]. These species trigger proteins and LPO via damaging the macromolecular cellular components of the cell membrane, inducing oxidative stress and starting cell apoptosis [49]. Antioxidants regulate the cellular oxidative stress that is induced via an inequality in the cellular production of ROS and reactive nitrogen species (RNS) [50]. Since the heart lacks antioxidant enzymes, this results in extensive destruction of the cardiac cellular mitochondrial membranes, nucleic acids, and endoplasmic reticulum [51].

Our investigation showed a marked elevation in cardiac nitric oxide NO levels in DOX-rats when compared with control rats (Fig 5), in agreement with previous research [52]. The capability of DOX to intercede the induction of NOS expression and NO release in the heart is the reason for the ascent in NO levels. Further, DOX causes a surge in e-NOS transcription and protein activity in cardiac endothelial cells by H_2O_2 and calcium influx triggering, leading to the synthesis of NO [53]. A recent study gives evidence of the upregulation of iNOS genes and protein expression in DOX-induced cardiomyopathy. The concomitant overabundance of NO and ROS yields excessive levels of peroxinitrite and RNS, which may invade and damage vital cellular biomolecules [54].

In our study, we investigated the protective effects of QU and QU-CHSNPs on DOX-induced cardiotoxicity and the underlying mechanisms of this protection [55]. As displayed in Fig 5, QU decreased NO levels with an even greater decrease in QU-CHSNPs. This may be because QU leads to the scavenging of free radicals, which decreases their interactions with nitric oxide and thus reduces the amount of damage [56]. The results suggest that QU provides cardiac protection against DOX by decreasing oxidative stress and damage. It is worth mentioning that the administration of QU-CHSNPs in normal rats showed a non-significant change when compared to the control, indicating safety.

Oxidative stress provides deleterious effects either by triggering LPO or by operating as a second messenger for primary free radicals that start LPO [57-58]. MDA levels were measured in the present study as an indicator for LPO [59]. In Fig 5, DOX administration caused a significant increase in MDA levels compared to the control, consistent with preceding research that employed an analogous drug regimen [60, 61, 62]. The initial targets of DOX-mediated free radical damage are cellular membranes that are rich in lipids susceptible to peroxidation. This radical damage produces stable and toxic aldehydes, such as MDA. These aldehydes can diffuse within the cell, or even cross the plasma membrane, and attack macromolecular targets far from where they were generated, thus acting as "second cytotoxic messengers." The treatment of DOX-injected rats with QU showed a decrease in MDA levels with QU-CHSNPs high pattern, Fig 5. The existing research supports the potency antioxidant activity of QU versus

DOX-induced oxidative stress in vivo, as evidenced by the inhibition of ROS generation and the reduction in MDA LPO activity, which corresponds with the findings [63].

Furthermore, our results confirmed that DOX decreased the antioxidant content and performance of non-enzymatic (GSH), enzymatic GPx, SOD, and glutathione-S-transferase (GST), significantly, as shown in Fig 5. These results are in accord with preceding reviews [64, 65, 66], which supported the competence of DOX to provide ROS and overthrow the antioxidant defence policy. Our results connected the devaluation in cardiac GSH content to the enhanced responses of the GSH metabolizing enzymes. The first enzyme is GPx, which catalyzes the disintegration of H_2O_2 and organic peroxides through its four selenium co-factors, using GSH as a reducing agent. The Fig 5 revealed a decline in GPx in the DOX-rats, and this was because of the mopping up of GPx by the free radicals generated by DOX [67]. The second enzyme is GST, which employs GSH in the conjugation of DOX toxic metabolites [68]. GST detoxifies xenobiotics, drugs, and carcinogens and supports cells against redox cycling and oxidative stress. The heart possesses low levels of GST and an overwhelming generation of free radicals by DOX may result in low GST levels higher than natural levels.

The administration of QU and QU-CHS enhanced the activities of the antioxidants GSH, GPx, SOD, and GST against DOX, in agreement with previous research [69]. Thus, QU scavenges for superoxide radicals and reduces myocardial damage. Indeed, evidence indicated that QU has cardioprotective properties because of its antioxidant activity. QU is an excellent metal chelator that chelates transition metals such as iron, which can initiate the formation of ROS. The scavenging of free radicals and chelating effects are both involved in its cardio-treatment and protective effects [21].

Lipids

Lipids play a role in cardiovascular disease complications. DOX interferes with the lipid metabolism, changing the lipid profile. In Fig 6, the levels of T. cholesterol, TG, LDL-c, and VLDL-c were found to increase in the DOX-rats, consistent with previous research [70, 71]. The increase in the cholesterol concentration could be because of a reduction in HDL levels, as HDLs transport cholesterol from tissues to the liver for catabolism. In this context, we observed decreased levels of HDLs in the DOX-rats. We attribute the elevation in TGs to the low activity of lipoprotein lipase. These changes in lipid levels may be due to enhanced lipid biosynthesis by the cardiac cyclic adenosine monophosphate [72]. Lipid-lowering drugs preserve the myocardium from DOX-induced toxicity. [73].

The administration of QU and QU-CHSNPs decreases the concentration of total cholesterol, TGs, VLDLs, and LDLs and increases the concentration of HDLs in the DOX-induced rats. QU and QU-CHSNPs were both effective at ameliorating cholesterol levels. Other studies have shown the effectiveness of QU in minimizing dyslipidemia [74]. Furthermore, QU has anti-hypercholesterolemia, antihypertensive, vasodilator, and anti-atherosclerotic properties [75]. The presented results suggest that QU has a talent for acting as a cardioprotective agent against DOX-induced cardiotoxicity.

CK-MB, AST, and LDH activities

This investigation showed that DOX-induced cardiotoxicity was manifested by a significant elevation in serum CK-MB, AST, and LDH activities (Fig 7), in agreement with previous research [76-77]. A possible explanation is the DOX induced damage of the cardiomyocyte membranes, releasing these entities from the cytoplasm into the plasma. Further, elevation of the cardiac enzyme function was found to be associated with histological degradation such as distinct necrosis of cardiomyocytes and inflammatory leukocytic infiltration into cardiac tissues [78-79]. In this study, the QU and QU-CHSNPs treatments lessened the CK-MB, AST, and LDH in the DOX-injected rats. Our results significantly reinforce the conclusion of preceding research [80], which showed that the QU pretreatments induced a substantial decline in the CK-MB, AST, and LDH activities when compared with the toxic control rats. This may be because of the protective effects of the QU in regulating the leakage of CK-MB, AST, and LDH. QU possesses free radical scavenging and antioxidant activities, which could justify its competence to defend the myocardium from DOX-induced damage by blocking the leakage of cardiac LDH, AST, and CK-MB isoenzymes [21]. Based on these results, QU and QU-CHSNPs retain potent cardioprotective effects against DOX-induced heart injury.

Cardiac troponin (c Tn-I)

c Tn-I level function is a sensitive and specific marker for myocardial cell injury. This contractile protein is not normally present in the serum and is released only after myocardial necrosis. Elevated troponin I levels predict the risks of both cardiac cell death and infarction following infarction [81]. In this study, the development of cardiotoxicity in the DOX group was also evidenced by elevated c Tn-I levels in the serum (Fig 7), which was in accordance with previous research [82]. However, the QU treatment reduced the c Tn-I levels in the serum, which was also in agreement with previous research [83]. These decreases of the c Tn-I level in the serum suggest that QU and QU-CHSNPs protects against DOX-induced cardiotoxicity in rats.

Cytokines (IL-1B, TNF-α and IL-10)

Inflammation participates in the pathogenesis of DOX-induced cardiotoxicity. It is fully cited that the overabundance of free radicals enhances the output of inflammatory mediators and triggers cardiac inflammatory processes [84]. The progressive increase of pro-inflammatory and a cytokine level within heart tissues was identified as a potential pathological indication for DOX-induced cardiomyopathy. The results, in line with previous investigations, support the idea that inflammation plays a fundamental part in the pathogenesis of DOX-induced cardiotoxicity. The current study found a significant increase in serum TNF- and IL-1B in the DOX group, which is consistent with previous findings [85, 86] (Fig 8). The principal underlying mechanism promoting this elevation in inflammatory markers is not yet understood. However, it is possible that heightened levels of ROS, impaired tissue antioxidant capacity, and subsequent LPO are provoking factors for these variations.

Indeed, it was declared that rises in inflammatory mediators interacted with heightened oxidative stress, which is considered to provoke inflammatory reactions through the activation of the NF-κB pathway, resulting in the transactivation of cytokines [85]. QU and QU-CHSNPs administration inhibited the

elevated TNF- in DOX-treated rats. In harmony with this finding, it has been shown that QU can inhibit NF-KB via its free radical scavenging and antioxidant activities [21]. According to this result, QU and QU-CHSNPs inhibit the elevated IL-1β in DOX-treated rats.

On the other hand, the results of this study have shown that DOX causes a significant decrease in serum anti-inflammatory cytokine IL-10 in DOX- rats (Fig 8), in agreement with previous research [87], while QU and QU-CHSNPs increased the IL-10 levels. The standing research asserted that QU has anti-inflammatory properties and acts by suppressing pro-inflammatory cytokines. While the mechanisms by which QU increases IL-10 levels are not clear [88].

Apoptotic markers

The oxidative stress generated by the DOX triggers many signalling pathways of cardiomyocyte apoptosis, including the activation of caspase-3 [85]. The caspase-3 protein is a cysteine-aspartic protease that is activated in apoptotic cells by the death ligand. The caspase-3 protein is thought to be a biomarker of cardiac tissue toxicity [89]. The present study showed that DOX causes a significant elevation of caspase-3 levels (Fig 8), in agreement with previous research [90]. Also, the results of this investigation agree with previous findings, which showed that DOX increases the levels of caspase-3, activates apoptosis by decreasing the expression of antiapoptotic proteins, and induces oxidative stress by increasing H_2O_2 production [91]. QU and QU-CHSNPs administration reduced the elevated caspase-3. These results are in accordance with previous research, which supports the hypothesis that the protection presented against DOX-induced cardiotoxicity by treatment with QU may involve the suppression of cardiac apoptosis [92].

Cardiac mRNA expression of annexin-V, NrF2 and PPAR-γ

The Annexin isoforms II, V, and VI are a particular group of membrane-associated, Ca2+-binding proteins that exist in heart tissue. Annexin V is present in both cardiomyocytes and non-myocytes and may play a part in regulating cellular ion fluxes, organization, and secretion. To determine alterations in the annexin V isoform that might arise in heart failure, we measured mRNA expression of this annexin. DOX administration caused a significant increase in cardiac annexin-V (Fig 9) compared with control, indicating heart failure. A possible explanation for this might be that DOX can disturb the homeostasis of intracellular calcium cycling in the heart, in agreement with previous research [93]. The DOX-rats treated with QU and QU-CHSNPs revealed a considerable decline in their cardiac annexin-V ascent levels, consistent with the preceding study [92]. It is essential to notice that QU-CHSNPs decreased the annexin-V elevation more than QU alone.

Nuclear factor erythroid 2 related factor 2 (Nrf2), a transcriptional factor, retains crucial protective effects against oxidative stress. In the oxidative stress stage, Nrf2 is triggered, enters the cell nucleus, stimulates antioxidant gene expression, and reduces oxidative damage. Preceding research showed that DOX-induced oxidative stress is correlated with cardiac damage [86]. In our study, DOX administration decreased active nuclear Nrf2 in the cardiac tissues (Fig 9), consistent with previous research [94]. The

upregulation of Nrf2 is a unique way to limit DOX-induced cardiac injury [86]. The current study proved that QU and QU-CHSNPS protect against DOX-induced cardiomyopathy by increasing NrF2 expression, which stimulates the synthesis of antioxidant defenses. Furthermore, QU has free radical scavenging and antioxidant properties [75].

Peroxisome proliferation-activated receptor gamma (PPAR-γ) is a nuclear receptor that regulates the transcription of several genes that are primarily involved in fatty acid and energy metabolism [95]. PPAR-γ is also present in a variety of cell types, including cardiomyocytes and vascular cells. PPAR-γ activation reduces the production of inflammatory cytokines, and there is growing evidence that PPAR-γ ligands have anti-inflammatory, antioxidative, and antiproliferative effects on cardiomyocytes [96]. DOX treatment significantly decreases PPAR-γ levels. These results suggest that PPAR-γ may help to protect rats from DOX-related heart injuries [97]. Moreover, our results have indicated that PPAR-γ levels were increased by the treatment with QU and QU-CHS (Fig. 9). We have concluded that quercetin increased PPAR-γ and reduced inflammation due to its anti-inflammatory properties [88].

Cardiac DNA fragmentation

In this investigation, the DNA fragmentation of cardiomyocytes was significantly high after the DOX administration (Fig 10), which is a sign of oxidative stress. The reason is that DOX promotes mitochondrial ROS production, which in turn damages cardiomyocyte DNA and triggers apoptosis [98-99]. QU and QU-CHSNPs showed a reduction in DNA fragmentation. This agrees with other research [67], which reported QU attenuates DOX-cardiotoxicity by reducing oxidative stress, ROS levels, and DNA damage to maintain heart cell viability. Our results were harmonious with another investigation, which confirmed that QU limited the pernicious effects of DOX and cyclophosphamide on the kidney and liver, obstructing peroxidative destruction [100].

Electron microscope and histopathology

Mitochondria are membrane-bound cells, their potential saved in adenosine triphosphate (ATP). One of the key managers in DOX-induced cardiotoxicity is mitochondria. The reason is that DOX suppresses mitochondrial synthesis, stimulates fission, and impairs mitochondrial function, ending with heart collapse. In this investigation, the mitochondrial determinants of DOX cardiotoxicity were assessed, and the results showed that the size, shape, and integrity of the mitochondria were lost (Fig 11 B), while the QU-CHS preserved their membrane integrity but seemed to be compact (Fig 11 C) not elongated like the control (Fig 11 A). Understanding the critical role of mitochondria in DOX-induced cardiomyopathy is critical to reduce the barriers that severely limit the clinical success of this life-saving anticancer therapy.

Considering the histological changes of the heart in normal rats, no histopathological alterations were observed, and a normal histological structure of the cardiac muscles could be found (Fig. 12A). Severe degenerative changes and necrosis of the cardiac muscles were accompanied by focal lymphocytic infiltration in the DOX-treated group (Fig. 12B). Treatment of DOX-administered rats with QU showed moderate hyalinosis of the cardiac muscles and focal lymphocytic infiltration (Fig 12C). Treatment of the

DOX-administered rats with QU-CHS was associated with mild to moderate degenerative changes of the cardiac muscles and minimal lymphocytic myocarditis (Fig 12D). Additionally, the normal group treated with QU-CHS showed minimal changes to the cardiac muscles and lymphocytic myocarditis (Fig 12E). In general, DOX administration caused severe histopathological lesions, which were characterized by severe inflammatory cell infiltration, hemorrhage, degeneration, and necrosis, and this was in agreement with previous research [101]. In this investigation, QU was found to have an anti-inflammatory effect as it improved the histopathological features of DOX-induced cardiotoxicity and decreased inflammation, degeneration, and necrosis of the myocardium, in agreement with others [102].

Overall, through the current study, one can see the protective effect of QU-CHSNPs was better than that of QU-free. An explanation for this may be that the QU encapsulation with CHSNPs could avoid enzymatic degradation in the gastrointestinal tract, limit the burst release, and sustain an adequate QU release rate pattern. Chitosan is a suitable absorption enhancer for poorly absorbable drugs because of its mucoadhesive properties, and it could boost the QU absorption across the intestinal mucosa, increasing its bioavailability. As was noted, the QU-CHSNPs has a positive surface charge, so it is possible to enter cardiac cells more rapidly through the endocytosis process when compared to QU-free. Another explanation is that the CHSNPs with high surface area could increase the loaded QU dose and enhance its therapeutic action.

Conclusion

The results indicated that QU and QU-CHSNPs have adequate preventive activity against doxorubicin-induced cardiotoxicity as supported by biochemical and histological findings. The QU-CHSNPs were extremely dominant in inhibiting the DOX-induced cardiac toxicities. These preventive effects may be mediated via suppression of oxidative and enhancement of antioxidant defence mechanisms in the heart.

Declarations

*Ethics approval and consent to participate

The authors followed the ethics of research, approved and consented to participate in this study. The Institutional Animal Care Committee of Beni-Suef University, Egypt, approved the entire conducted procedures (BSU/2018/11/17).

All the authors consent and understand that their participation is voluntary and that they are free to withdraw at any time, without giving a reason and without cost. All authors understand that they will be given a copy of this consent form. All authors voluntarily agree to take part in this study.

*Consent for publication

The authors consent this manuscript for publication

***Availability of data and material**

The authors emphasize the availability of data and materials

***Competing interests**

The authors confirm no competing interests

***Funding**

The present study was supported by individual funding

***Acknowledgements**

The authors are thankful to all members at Materials Science and nanotechnology Department, Faculty of Postgraduate Studies for Advanced Sciences (PSAS), Beni-Suef University, Egypt. and Dr. El-Shaymaa El-Nahass, Associate Prof. of Histopathology, Pathology Department, Faculty of Veterinary Medicine, Beni-Suef University and Egypt for help in examining and determining the lesions in the heart histological stained sections.

***Author Contributions**

Dr. Elshahawy conceived the idea for biomedical application, Dr. Elshahawy, Asmaa. G. Soliman, and Mohamed Abdel-Gabbar participated in the study design. Dr. Elshahawy, Asmaa. G. Soliman and Zienab E. Eldin prepared the materials. Dr. Elshahawy, Asmaa. G. Soliman, and Mohamed Abdel-Gabbar conducted the bio section. Dr. Elshahawy, Asmaa. G. Soliman wrote the manuscript. Dr. Basant Mahmoud revised the manuscript. All the authors revised the manuscript and approved the final version to be published, and agreed to be accountable for all aspects of the work in ensuring that questions related to the accuracy or integrity of any part of the work are appropriately investigated and resolved.

References

1. Iqubal, A., et al., *Clinical updates on drug-induced cardiotoxicity.* International Journal of Pharmaceutical Sciences and Research, 2018. 9: p. 16-26.
2. Cappetta, D., et al., *Oxidative stress and cellular response to doxorubicin: a common factor in the complex milieu of anthracycline cardiotoxicity.* Oxidative medicine and cellular longevity, 2017. 2017.
3. Pugazhendhi, A., et al., *Toxicity of Doxorubicin (Dox) to different experimental organ systems.* Life sciences, 2018. 200: p. 26-30.
4. Zhao, L., et al., *MicroRNA-140-5p aggravates doxorubicin-induced cardiotoxicity by promoting myocardial oxidative stress via targeting Nrf2 and Sirt2.* Redox biology, 2018. 15: p. 284-296.
5. C Pereira, G., et al., *Drug-induced cardiac mitochondrial toxicity and protection: from doxorubicin to carvedilol.* Current pharmaceutical design, 2011. 17(20): p. 2113-2129.

6. Hashish, F.E., et al., *Possible protective effects of quercetin on doxorubicin-induced cardiotoxicity in rats.* Menoufia Medical Journal, 2021. 34(1): p. 333.
7. Hussain, T., et al., *Flavonoids and type 2 diabetes: Evidence of efficacy in clinical and animal studies and delivery strategies to enhance their therapeutic efficacy.* Pharmacological research, 2020. 152: p. 104629.
8. Ferenczyova, K., B. Kalocayova, and M. Bartekova, *Potential implications of quercetin and its derivatives in cardioprotection.* International journal of molecular sciences, 2020. 21(5): p. 1585.
9. Nathiya, S., M. Durga, and T. Devasena, *Preparation, physico-chemical characterization and biocompatibility evaluation of quercetin loaded chitosan nanoparticles and its novel potential to ameliorate monocrotophos induced toxicity.* Dig. J. Nanomater. Bios, 2014. 9: p. 1603-13.
10. Ertuğ, P.U., et al., *Comparative study of the quercetin, ascorbic acid, glutathione and superoxide dismutase for nitric oxide protecting effects in mouse gastric fundus.* European journal of pharmacology, 2013. 698(1-3): p. 379-387.
11. Castillo, R.L., et al., *Quercetin prevents diastolic dysfunction induced by a high-cholesterol diet: role of oxidative stress and bioenergetics in hyperglycemic rats.* Oxidative medicine and cellular longevity, 2018. 2018.
12. Li, Y., et al., *Quercetin, inflammation and immunity.* Nutrients, 2016. 8(3): p. 167.
13. Choudhary, A., et al., *Quercetin loaded chitosan tripolyphosphate nanoparticles accelerated cutaneous wound healing in Wistar rats.* European journal of pharmacology, 2020. 880: p. 173172.
14. Zhao, L.-M., et al., *Preparation and application of chitosan nanoparticles and nanofibers.* Brazilian Journal of Chemical Engineering, 2011. 28: p. 353-362.
15. Fan, W., et al., *Formation mechanism of monodisperse, low molecular weight chitosan nanoparticles by ionic gelation technique.* Colloids and surfaces B: Biointerfaces, 2012. 90: p. 21-27.
16. Xu, Y., et al., *Preparation of dual crosslinked alginate–chitosan blend gel beads and in vitro controlled release in oral site-specific drug delivery system.* International Journal of Pharmaceutics, 2007. 336(2): p. 329-337.
17. Luque-Alcaraz, A.G., et al., *Characterization and antiproliferative activity of nobiletin-loaded chitosan nanoparticles.* Journal of Nanomaterials, 2012. 2012.
18. Tamilselvan, N. and C.V. Raghavan, *Formulation and characterization of anti alzheimer's drug loaded chitosan nanoparticles and its in vitro biological evaluation.* Journal of young pharmacists, 2015. 7(1): p. 28.
19. Rashedi, J., et al., *Anti-tumor effect of quercetin loaded chitosan nanoparticles on induced colon cancer in wistar rats.* Advanced Pharmaceutical Bulletin, 2019. 9(3): p. 409.
20. Raj, L.A., et al., *Preparation and characterization of BSA and chitosan nanopartices for sustainable delivery system for quercetin.* Journal of Applied Pharmaceutical Science, 2015. 5(7): p. 001-005.
21. Matook, A.I., et al., *Potential protective role of quercetin against chronic doxorubicin induced cardiotoxicity in rats.* EL-mina med. bull, 2012. 23(2).

22. Ibrahim, M.A., et al., *Angiotensin-converting enzyme inhibition and angiotensin AT1-receptor antagonism equally improve doxorubicin-induced cardiotoxicity and nephrotoxicity.* Pharmacological research, 2009. 60(5): p. 373-381.
23. Friedman, R.B. and D.S. Young, *Effects of disease on clinical laboratory tests, 3th ed. AACC press.* 1997.
24. Burtis, C.A., E.R. Ashwood, and D.E. Bruns, *Tietz textbook of clinical chemistry and molecular diagnostics, 4th ed. WBSa unders Co.* 2005.
25. Witt, I. and C. Trendelenburg, *Gemeinsame Studie zur Erstellung von Richtwerten für klinisch-chemische Kenngrößen im Kindesalter.* Journal of clinical chemistry and clinical biochemistry. Zeitschrift fur klinische Chemie und klinische Biochemie, 1982. 20:: p. 235-242.
26. Young, D., *Effects of disease on Clinical Lab.* Tests, 4th ed AACC, 2001.
27. Friedewald, W.T., *levy, RI; and Fredrickson, DS (1972). Estimation of the Concentration of low–density lipoprotein cholesterol in plasma without use of Preparative ultracentrifuge.* Clin chem. 18(6): p. 499-502.
28. Tietz, N.W., P.R. Finley, and E. Pruden, *Clinical guide to laboratory tests*. Vol. 624. 1995: WB Saunders company Philadelphia.
29. Habig, W., M. Pabst, and W. Jakoby, *Biological assay kit measures total GST activity.* WJ Biol. Chem, 1974. 249: p. 7130-7139.
30. Paglia, D.E. and W.N. Valentine, *Studies on the quantitative and qualitative characterization of erythrocyte glutathione peroxidase.* The Journal of laboratory and clinical medicine, 1967. 70(1): p. 158-169.
31. Beutler, E., O. Duron, and M. Kelly, *Evaluation of glutathione level in extra-cellular fluid.* J Lab Clin Med, 1963. 61: p. 882-7.
32. Ohkawa, H., N. Ohishi, and K. Yagi, *Assay for lipid peroxides in animal tissues by thiobarbituric acid reaction.* Analytical biochemistry, 1979. 95(2): p. 351-358.
33. Montogomery, H. and J. Dymock, *The determination of nitrite in water: colorimetric method of nitric oxide assay.* Analyst, 1961. 86: p. 414.
34. Abdel-Aziz, M.M., M. Yosri, and B.H. Amin, *Control of imipenem resistant-Klebsiella pneumoniae pulmonary infection by oral treatment using a combination of mycosynthesized Ag-nanoparticles and imipenem.* Journal of radiation research and applied sciences, 2017. 10(4): p. 353-360.
35. Abdel-Moneim, A., et al., *Novel polydatin-loaded chitosan nanoparticles for safe and efficient type 2 diabetes therapy: In silico, in vitro and in vivo approaches.* International Journal of Biological Macromolecules, 2020. 154: p. 1496-1504.
36. Stachurski, Z.H., *On structure and properties of amorphous materials.* Materials, 2011. 4(9): p. 1564-1598.
37. Ritchie, A.W., et al., *Reversed crystal growth of rhombohedral calcite in the presence of chitosan and gum arabic.* CrystEngComm, 2013. 15(47): p. 10266-10271.

38. Abd El-Rahmanand, S.N. and S. Suhailah, *Quercetin nanoparticles: Preparation and characterization.* Indian Journal of Drugs, 2014. 2(3): p. 96-103.
39. Zhao, X., et al., *Recrystallization and micronization of taxol using the supercritical antisolvent (SAS) process.* Industrial & engineering chemistry research, 2012. 51(28): p. 9591-9597.
40. Muller, R., *Drug nanocrystals of poorly soluble drugs.* Encyclopedia of nanoscience and nanotechnology, 2004: p. 627-638.
41. Zhang, J.-Y., et al., *Preparation of amorphous cefuroxime axetil nanoparticles by controlled nanoprecipitation method without surfactants.* International Journal of Pharmaceutics, 2006. 323(1-2): p. 153-160.
42. Lustriane, C., et al., *Effect of chitosan and chitosan-nanoparticles on post harvest quality of banana fruits.* Journal of Plant Biotechnology, 2018. 45(1): p. 36-44.
43. Sarkar, S.D., et al., *Physico-chemical/biological properties of tripolyphosphate cross-linked chitosan based nanofibers.* Materials Science and Engineering: C, 2013. 33(3): p. 1446-1454.
44. Ha, J.-H., et al., *Albumin release from bioerodible hydrogels based on semi-interpenetrating polymer networks composed of poly (ϵ-caprolactone) and poly (ethylene glycol) macromer.* Journal of controlled release, 1997. 49(2-3): p. 253-262.
45. Tacar, O., P. Sriamornsak, and C.R. Dass, *Doxorubicin: an update on anticancer molecular action, toxicity and novel drug delivery systems.* Journal of pharmacy and pharmacology, 2013. 65(2): p. 157-170.
46. Songbo, M., et al., *Oxidative stress injury in doxorubicin-induced cardiotoxicity.* Toxicology letters, 2019. 307: p. 41-48.
47. Al-Harthi, S.E., et al., *Amelioration of doxorubicin-induced cardiotoxicity by resveratrol.* Molecular medicine reports, 2014. 10(3): p. 1455-1460.
48. Ahmed, M., *The protective effect of ginger (Zingiber officinale) against adriamycin-induced hepatotoxicity in rats: histological study.* Life Sci J, 2013. 10(1): p. 1412-1422.
49. Ayla, S., et al., *Doxorubicin induced nephrotoxicity: protective effect of nicotinamide.* International journal of cell biology, 2011. 2011.
50. Mahmoud, A., et al., *Characterization of Ulva fasciata ethanolic extract-mediated biosynthesized silver nanoparticles and evaluation of their nephrocadiopreventive effects in doxorubicin-injected wistar rats.* Adv. Anim. Vet. Sci, 2020. 8(s2): p. 98-111.
51. Kelleni, M.T., E.F. Amin, and A.M. Abdelrahman, *Effect of metformin and sitagliptin on doxorubicin-induced cardiotoxicity in rats: impact of oxidative stress, inflammation, and apoptosis.* Journal of toxicology, 2015. 2015.
52. Saad, S.Y., T.A. Najjar, and M. Alashari, *Cardiotoxicity of doxorubicin/paclitaxel combination in rats: effect of sequence and timing of administration.* Journal of Biochemical and Molecular Toxicology, 2004. 18(2): p. 78-86.

53. Goetz, R.M., et al., *Estradiol induces the calcium-dependent translocation of endothelial nitric oxide synthase.* Proceedings of the National Academy of Sciences, 1999. 96(6): p. 2788-2793.
54. Ibrahim, S.S., et al., *Role of selenium in attenuating cardiac and hepatic damages induced by the antitumor agent, doxorubicin.* Life Sci J, 2011. 8: p. 1-12.
55. Chen, X., et al., *Quercetin protects cardiomyocytes against doxorubicin-induced toxicity by suppressing oxidative stress and improving mitochondrial function via 14-3-3γ.* Toxicology Mechanisms and Methods, 2019. 29(5): p. 344-354.
56. Baghel, S.S., et al., *A review of quercetin: antioxidant and anticancer properties.* World J Pharm Pharmaceutical Sci, 2012. 1(1): p. 146-160.
57. Nandakumar, N., et al., *Hesperidin, a natural citrus flavonoglycoside, normalizes lipid peroxidation and membrane bound marker enzymes in 7, 12-Dimethylbenz (a) anthracene induced experimental breast cancer rats.* Biomedicine & Preventive Nutrition, 2011. 1(4): p. 255-262.
58. Jaganjac, M., et al., *Reactive aldehydes–second messengers of free radicals in diabetes mellitus.* Free Radical Research, 2013. 47(sup1): p. 39-48.
59. Korkina, L.G. and I.B. Afanas' Ev, *Antioxidant and chelating properties of flavonoids.* Advances in pharmacology, 1996. 38: p. 151-163.
60. Kim, S.H., et al., *Comparision of doxorubicin-induced cardiotoxicity in the ICR mice of different sources.* Laboratory animal research, 2017. 33(2): p. 165-170.
61. Elberry, A.A., et al., *Cranberry (Vaccinium macrocarpon) protects against doxorubicin-induced cardiotoxicity in rats.* Food and chemical toxicology, 2010. 48(5): p. 1178-1184.
62. Balachandar, A., K. Malarkodi, and P. Varalakshmi, *Protective role of DLa-lipoic acid against adriamycin-induced cardiac lipid peroxidation.* Human & experimental toxicology, 2003. 22(5): p. 249-254.
63. Dong, Q., et al., *Quercetin attenuates doxorubicin cardiotoxicity by modulating B mi-1 expression.* British journal of pharmacology, 2014. 171(19): p. 4440-4454.
64. Hozayen, W.G., H.S. Abou Seif, and S. Amin, *Protective effects of ruitn and/or hesperidin against doxorubicin-induced hepatotoxicity.* Int J Clin Nutr, 2014. 2(1): p. 11-7.
65. QuanJun, Y., et al., *Protective effects of dexrazoxane against doxorubicin-induced cardiotoxicity: a metabolomic study.* PloS one, 2017. 12(1): p. e0169567.
66. Mahmoud, H., et al., *Effects of rutin and quercetin on doxorubicin-induced renocardiotoxicity in male Wistar rats.* Advances in Animal and Veterinary Sciences, 2020. 8(4): p. 2020370-384.
67. Omóbòwálé, T.O., et al., *Ameliorative effect of gallic acid on doxorubicin-induced cardiac dysfunction in rats.* Journal of basic and clinical physiology and pharmacology, 2018. 29(1): p. 19-27.
68. Ibrahim, S.S., M.A. Barakat, and H. Helmy, *Modulating effect of carvedilol on doxorubicin-induced cardiomyopathy and hepatic damage.* J Am Sci, 2010. 6(12): p. 20-32.
69. Arafa, H.M., M.F. Abd-Ellah, and H.F. Hafez, *Abatement by naringenin of doxorubicin-induced cardiac toxicity in rats.* Journal of the Egyptian national cancer institute, 2005. 17(4): p. 291-300.

70. Chennuru, A. and M.T. Saleem, *Antioxidant, lipid lowering, and membrane stabilization effect of sesamol against doxorubicin-induced cardiomyopathy in experimental rats.* BioMed research international, 2013. 2013.
71. Mubarak, S., et al., *Cardioprotective effect of date palm against doxorubicin-induced cardiotoxicity.* Asian J Pharm Clin Res, 2018. 11(7): p. 141-146.
72. Sakthivel, K., et al., *Cardioprotective and antioxidant potential of Scilla hyacinthina.* Journal of Biological Sciences, 2013. 13(5): p. 313.
73. Schimmel, K.J., et al., *Cardiotoxicity of cytotoxic drugs.* Cancer treatment reviews, 2004. 30(2): p. 181-191.
74. Aziz, T.A., *Cardioprotective Effect of Quercetin and Sitagliptin in Doxorubicin-Induced Cardiac Toxicity in Rats.* Cancer Management and Research, 2021. 13: p. 2349.
75. Sharma, A., et al., *Modulation of Nrf2 by quercetin in doxorubicin-treated rats.* Heliyon, 2020. 6(4): p. e03803.
76. Ahmed, O.M., M.B. Ashour, and A.S. Abd El-Fattah, *The Preventive effects of navel orange peel ethanolic extract and naringin on doxorubicin-induced nephrocardiotoxicity in male albino rats.* Indo Am. J. Pharm. Res, 2017. 7(07): p. 109-117.
77. Ahmed, O.M., et al., *Effects of green tea infusion and epicatechin on doxorubicin-induced renocardiotoxicity in male albino rats.* IJPSR, 2019. 10(5): p. 1000-1014.
78. Chen, P.Y., et al., *Protective effect of Co-enzyme Q10 On doxorubicin-induced cardiomyopathy of rat hearts.* Environmental toxicology, 2017. 32(2): p. 679-689.
79. Nimbal, S. and B. Koti, *Article Details Effect of Ethanolic Extract Fractions of Rosa centifolia in Doxorubicin-induced Myocardial Toxicity in Albino Rats.* 2018.
80. Nazmi, A.S., et al., *Protective effects of Bombyx mori, quercetin and benazepril against doxorubicin induced cardiotoxicity and nephrotoxicity.* Journal of Saudi Chemical Society, 2016. 20: p. S573-S578.
81. Afroz, R., et al., *Sundarban honey confers protection against isoproterenol-induced myocardial infarction in Wistar rats.* BioMed Research International, 2016. 2016.
82. Atas, E., et al., *Cardiac troponin-I, brain natriuretic peptide and endothelin-1 levels in a rat model of doxorubicin-induced cardiac injury.* Journal of cancer research and therapeutics, 2015. 11(4): p. 882.
83. Yaseen, A.E.-R.A., et al., *Potential protective effects of trimetazidine and quercetin on isoprenaline-induced myocardial infarction in rats.* Menoufia Medical Journal, 2017. 30(4): p. 1110.
84. Aziz, M.M., et al., *Protective effects of olmesartan and l-carnitine on doxorubicin-induced cardiotoxicity in rats.* Canadian journal of physiology and pharmacology, 2020. 98(4): p. 183-193.
85. Shaker, R.A., et al., *Enoxaparin attenuates doxorubicin induced cardiotoxicity in rats via interfering with oxidative stress, inflammation and apoptosis.* BMC Pharmacology and Toxicology, 2018. 19(1): p. 1-10.

86. Yang, H.-B., et al., *Selenium Attenuates Doxorubicin-Induced Cardiotoxicity Through Nrf2-NLRP3 Pathway.* Biological Trace Element Research, 2021: p. 1-9.
87. Pecoraro, M., et al., *Inflammatory mediators in a short-time mouse model of doxorubicin-induced cardiotoxicity.* Toxicology and applied pharmacology, 2016. 293: p. 44-52.
88. Mkhize, N.V.P., L. Qulu, and M.V. Mabandla, *The effect of quercetin on pro-and anti-inflammatory cytokines in a prenatally stressed rat model of febrile seizures.* Journal of experimental neuroscience, 2017. 11: p. 1179069517704668.
89. Al-Kuraishy, H. and R. Hussein, *Caspase-3 levels (CASP-3) in doxorubicin induced-cardiotoxicity: role of metformin pretreatment.* Research Journal of Oncology, 2017. 1(1).
90. Dash, S.K., et al., *Self-assembled betulinic acid protects doxorubicin induced apoptosis followed by reduction of ROS–TNF-α–caspase-3 activity.* Biomedicine & Pharmacotherapy, 2015. 72: p. 144-157.
91. Anghel, N., et al., *Acute cardiotoxicity induced by doxorubicin in right ventricle is associated with increase of oxidative stress and apoptosis in rats.* Histology and histopathology, 2017. 33(4): p. 365-378.
92. Chen, J.-Y., R.-Y. Hu, and H.-C. Chou, *Quercetin-induced cardioprotection against doxorubicin cytotoxicity.* Journal of biomedical science, 2013. 20(1): p. 1-11.
93. Zhang, X., et al., *Rosmarinic acid alleviates cardiomyocyte apoptosis via cardiac fibroblast in doxorubicin-induced cardiotoxicity.* International journal of biological sciences, 2019. 15(3): p. 556.
94. El-Agamy, D.S., et al., *Pristimerin protects against doxorubicin-induced cardiotoxicity and fibrosis through modulation of Nrf2 and MAPK/NF-kB signaling pathways.* Cancer management and research, 2019. 11: p. 47.
95. Ivanova, E.A., et al., *Peroxisome proliferator-activated receptor (PPAR) gamma in cardiovascular disorders and cardiovascular surgery.* Journal of cardiology, 2015. 66(4): p. 271-278.
96. Hasegawa, H., H. Takano, and I. Komuro, *Therapeutic Implications of PPAR in Cardiovascular Diseases.* PPAR research, 2010. 2010.
97. Yan, J., et al., *Piperine Alleviates Doxorubicin-Induced Cardiotoxicity via Activating PPAR-γ in Mice.* PPAR research, 2019. 2019.
98. Francis, A. and Y. Nayak, *Modulation of Doxorubicin-Induced Cardiotoxicity by Averrhoa bilimbi extract.* Journal of Young Pharmacists, 2017. 9(1).
99. Zanwar, A.A., M.V. Hegde, and S.L. Bodhankar, *Protective role of concomitant administration of flax lignan concentrate and omega-3-fatty acid on myocardial damage in doxorubicin-induced cardiotoxicity.* Food Science and Human Wellness, 2013. 2(1): p. 29-38.
100. Kocahan, S., et al., *Protective effect of quercetin against oxidative stress-induced toxicity associated with doxorubicin and cyclophosphamide in rat kidney and liver tissue.* Iranian journal of kidney diseases, 2017. 11(2): p. 124.
101. Iqbal, M., et al., *Protective effects of telmisartan against acute doxorubicin-induced cardiotoxicity in rats.* Pharmacological reports, 2008. 60(3): p. 382.

102. Matouk, A.I., et al., *Quercetin augments the protective effect of losartan against chronic doxorubicin cardiotoxicity in rats.* Environmental toxicology and pharmacology, 2013. 36(2): p. 443-450.

Figures

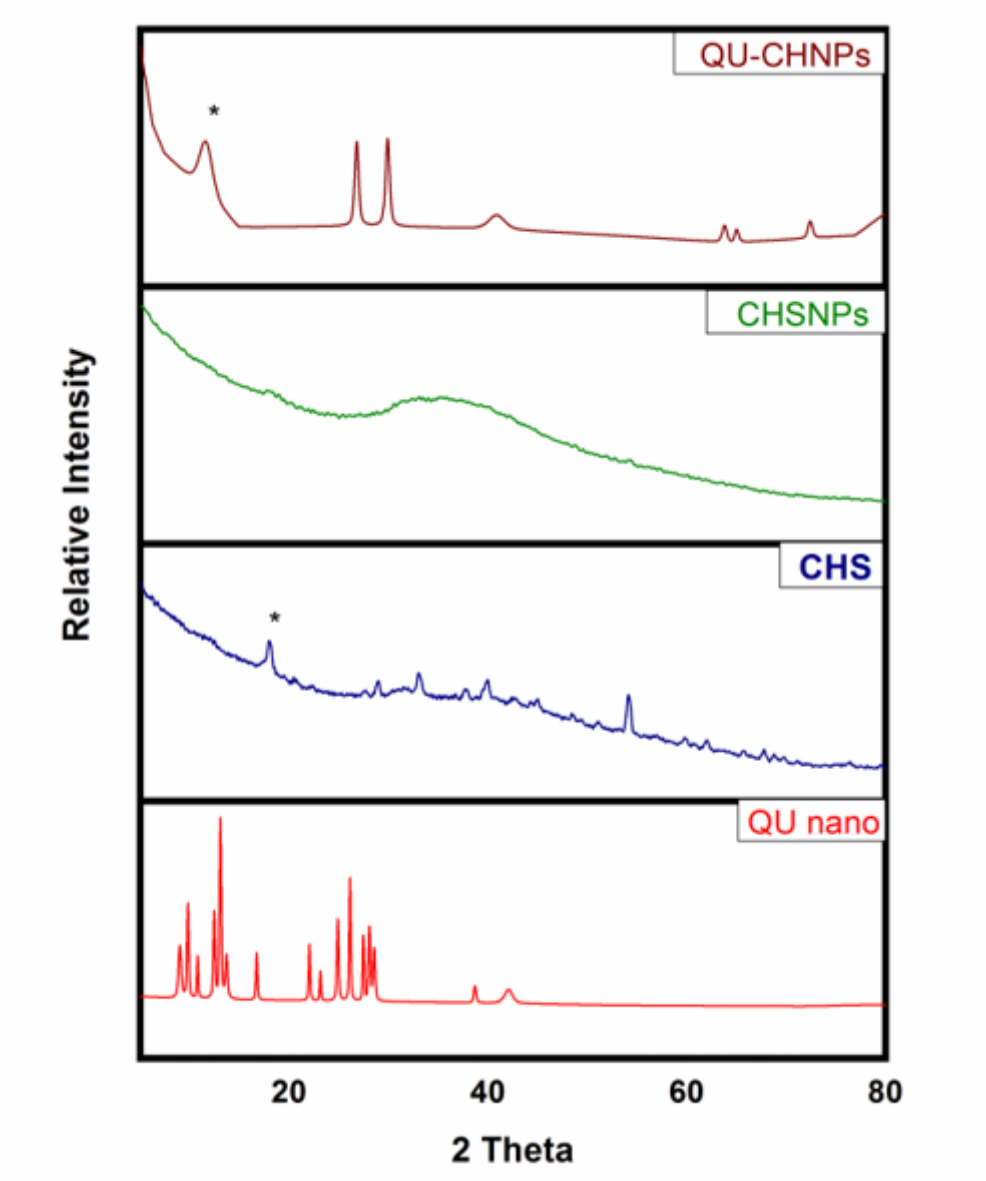

Figure 1

(A) XRD of QU nano, CHS, CHSNPs, and QU-CHSNPs over a 2θ range. The spectra showed languid changes in the shape, position of the diffracted signals, and relative integrated intensity of the diffracted peaks, confirming QU loading on CHSNPs.

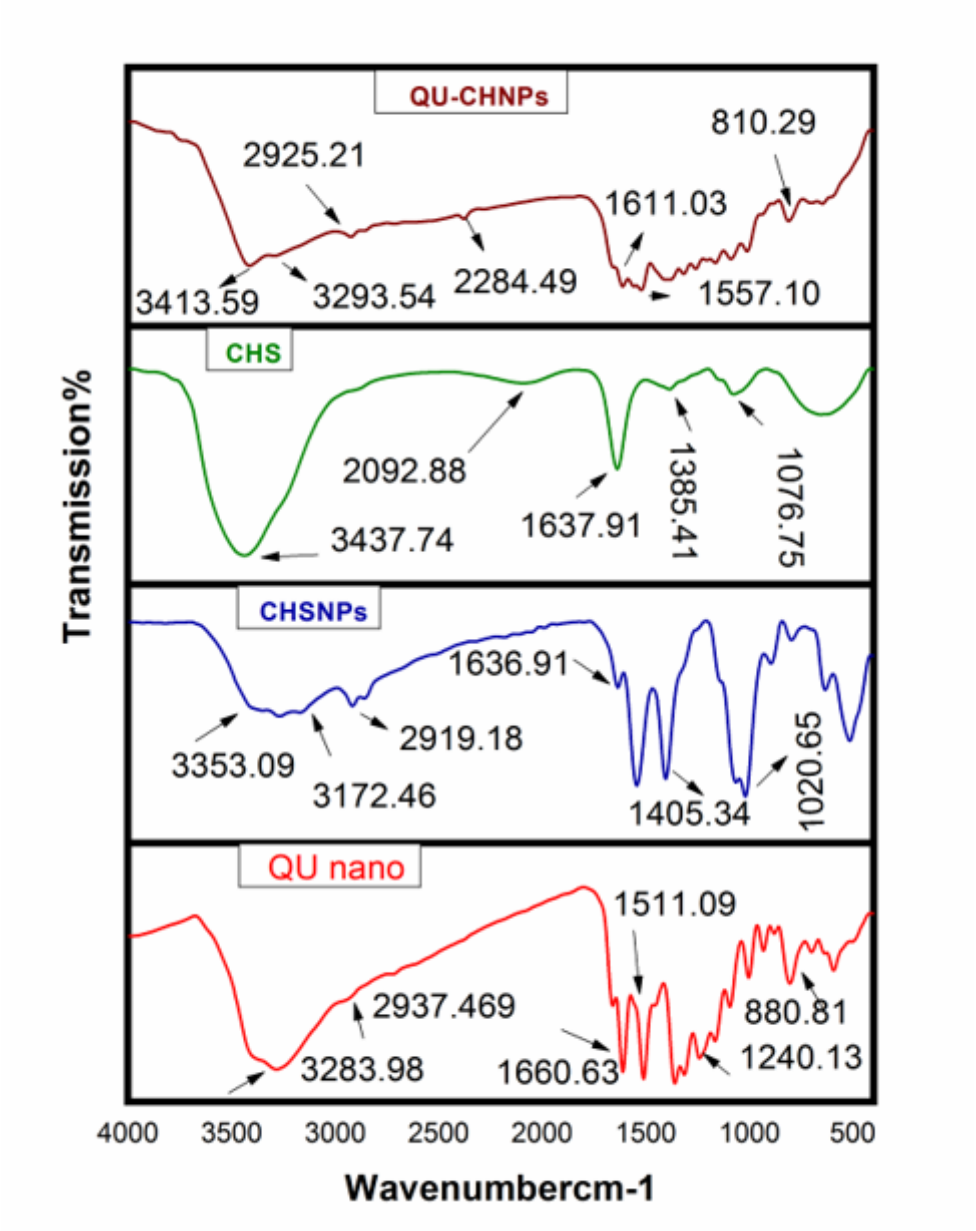

Figure 2

FTIR of QU nano, CHS, CHSNPs, and QU-CHSNPs, the QU-CHSNP peak patterns and positions varied significantly. These variations reflected interaction between CHSNPs and QU nano, confirming the loading process.

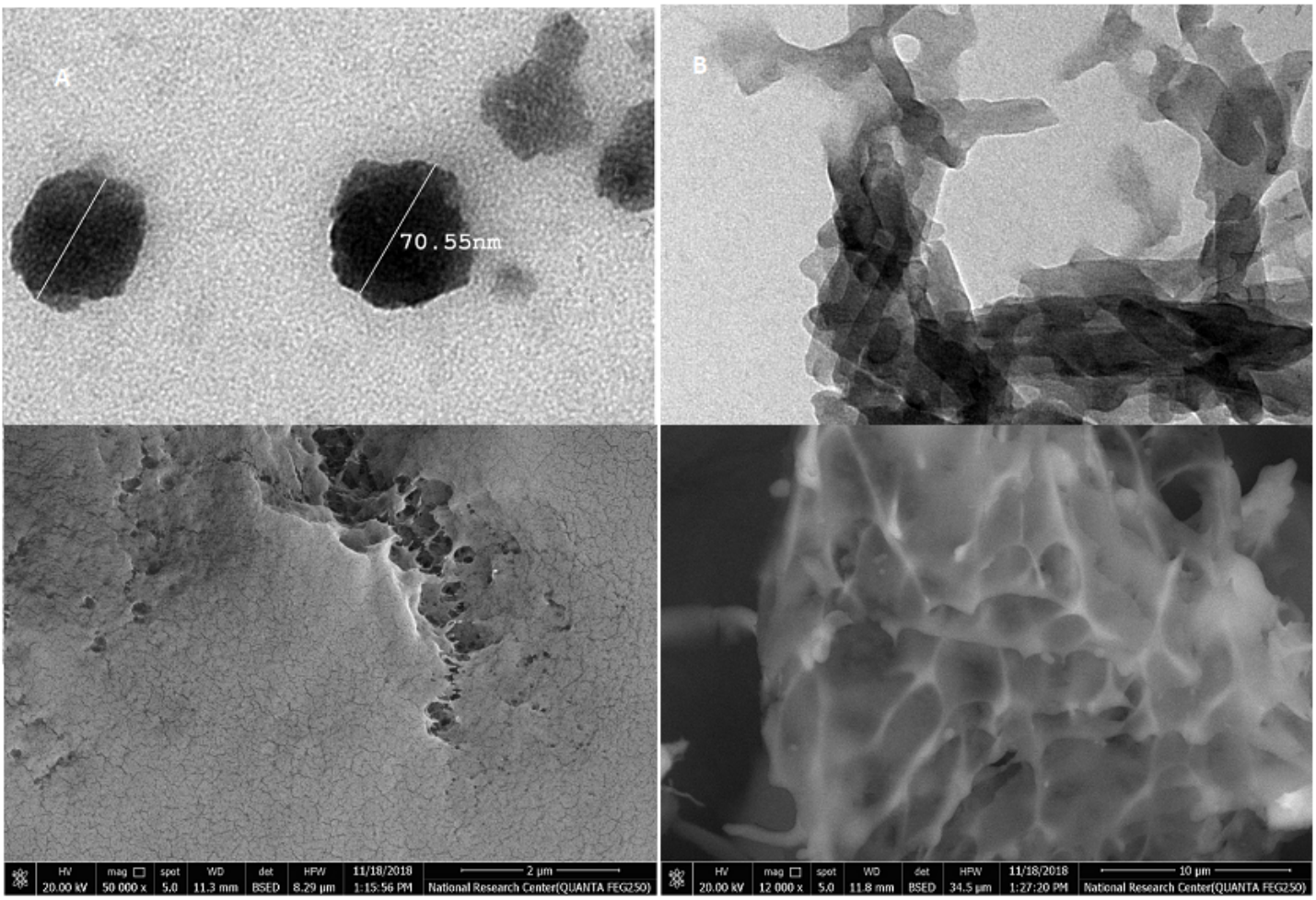

Figure 3

(A) HRTEM images of the spherical shape of the prepared CHSNPs with an average particle size of approximately 50 nm, (B) stacked clusters of the prepared QU-CHSNPs, (C) SEM image of CHSNPs with a non-homogeneous, rough, and irregular surface texture; (D) SEM image of QU-CHSNPs with a smooth surface pattern and pineapple morphology.

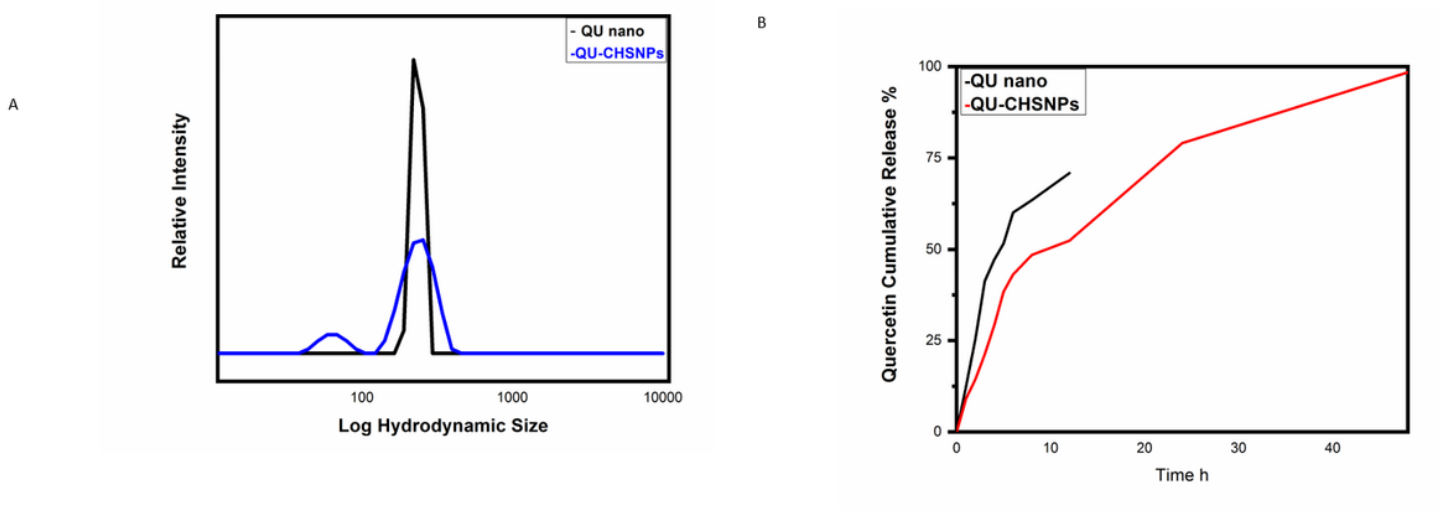

Figure 4

(A) QU nano and QU-CHSNP hydrodynamic size and size distribution, The polydispersity index of QU nano indicated a narrow width and a homogeneous size distribution, while that of QU-CHSNPs displayed a wide width and a heterogeneous size distribution. (B) 48-hour in vitro release profile of QU-CHSNPs versus free Quercetin Nano at pH 6.8 and 37°C. The results are averages (n = 3). Because of the slow diffusion of QU from the CHSNPs matrix, free QU had a lower cumulative drug percent than QU-CHSNPs, confirming a pattern of sustained release.

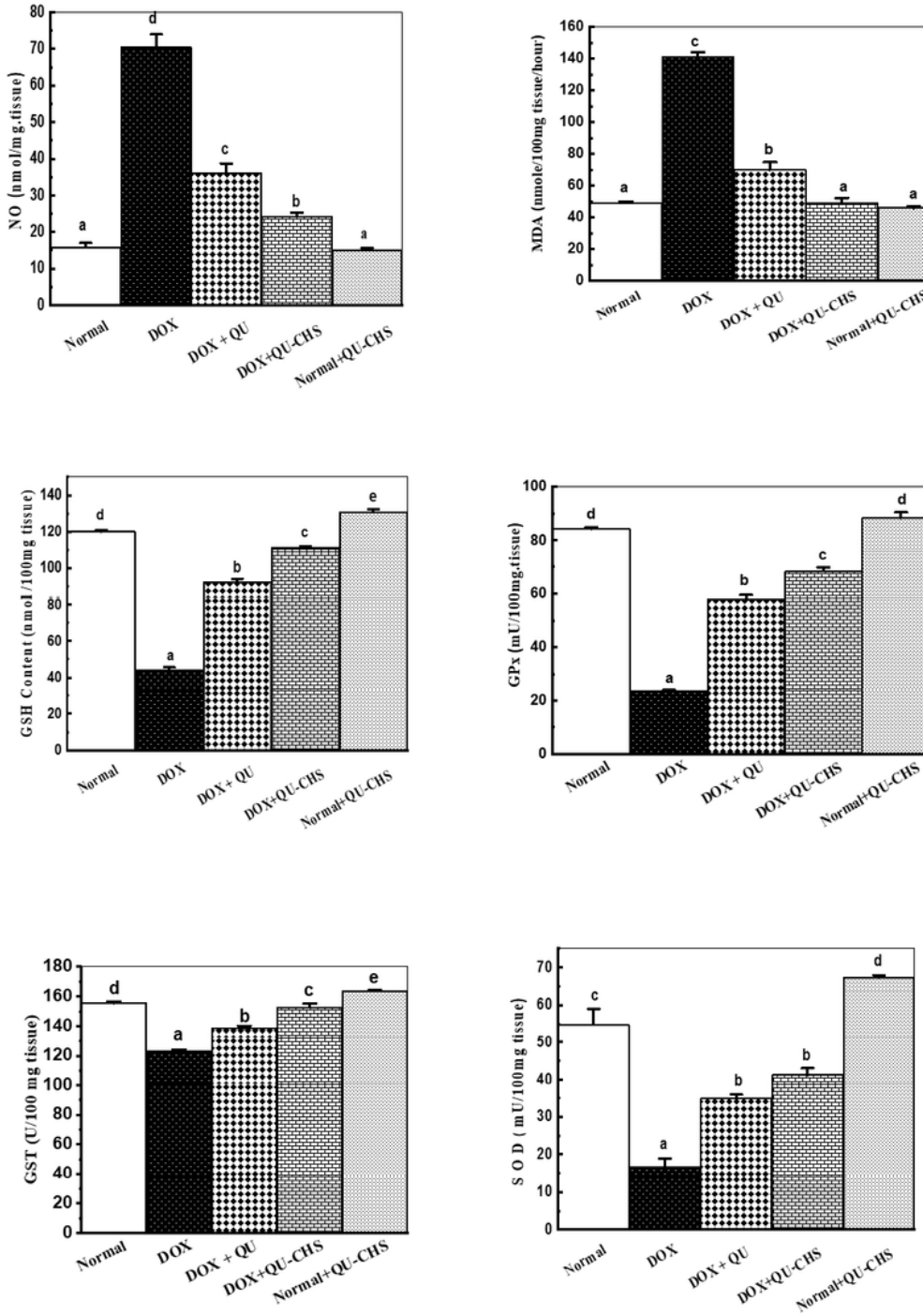

Figure 5

effect of QU and QU-CHSNPs on heart NO, MDA, GSH, GPX, GST, and SOD in normal control and DOX-administered rats. The data are presented as mean SE. The number of samples in each group is six. *P* 0.001 for F-probability values that share the same superscript symbol is not significantly different. Glutathione content (GSH), Glutathione peroxidase (GPx), Glutathione-S-transferase (GST), Superoxide

dismutase (SOD), DOX (Doxorubicin), QU (Quercetin), QU-CHS (QU-loaded CHSNPs), DOX (Doxorubicin), QU-CHS (QU-loaded CHSNPs),

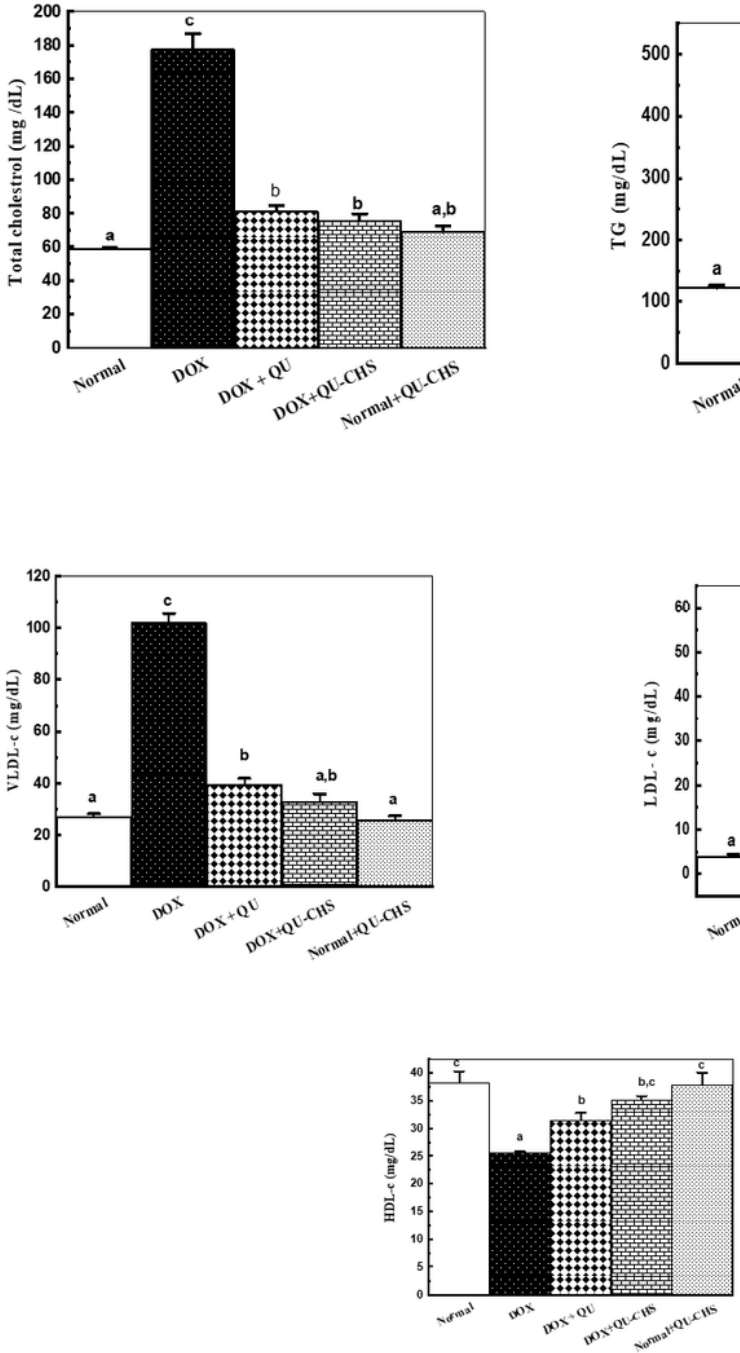

Figure 6

displays effect of QU and QU-CHSNPs on the serum lipid profile of normal control and DOX-administered rats. Data are expressed as Mean ± SE. Numbers of samples in each group is six. F-probability: P<0.001

values that share the same superscript symbol, are not significantly different. Low- density lipoprotein-cholesterol (LDL-c), Very-low -density lipoprotein-cholesterol (VLDL-c), High density lipoprotein-cholesterol (HDL-c), DOX (Doxorubicin), QU (Quercetin), QU-CHS (QU-loaded CHSNPs)

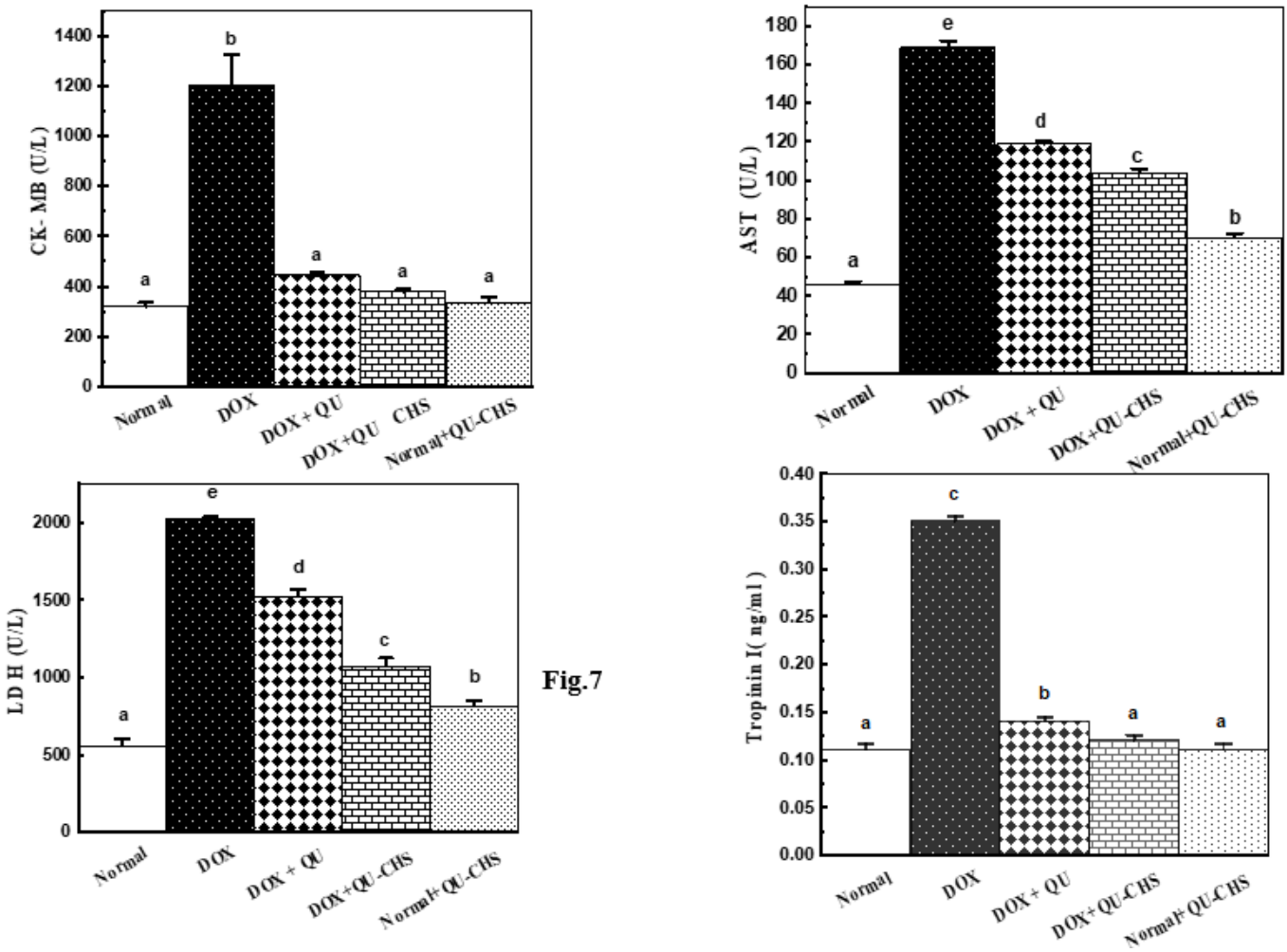

Fig.7

Figure 7

The effect of QU and QU-CHSNPs on serum Troponin-I, AST, LDH, and CK-MB activities in normal and DOX-treated rats. The data are presented as mean SE. The number of samples in each group is six. F-probability: P<0.001 values that share the same superscript symbol are not significantly different. Aspartate aminotransferase (AST), lactate dehydrogenase (LDH), Creatine Kinase-MB (CK-MB), DOX (Doxorubicin), QU (Quercetin), QU-CHS (QU-loaded CHSNPs)

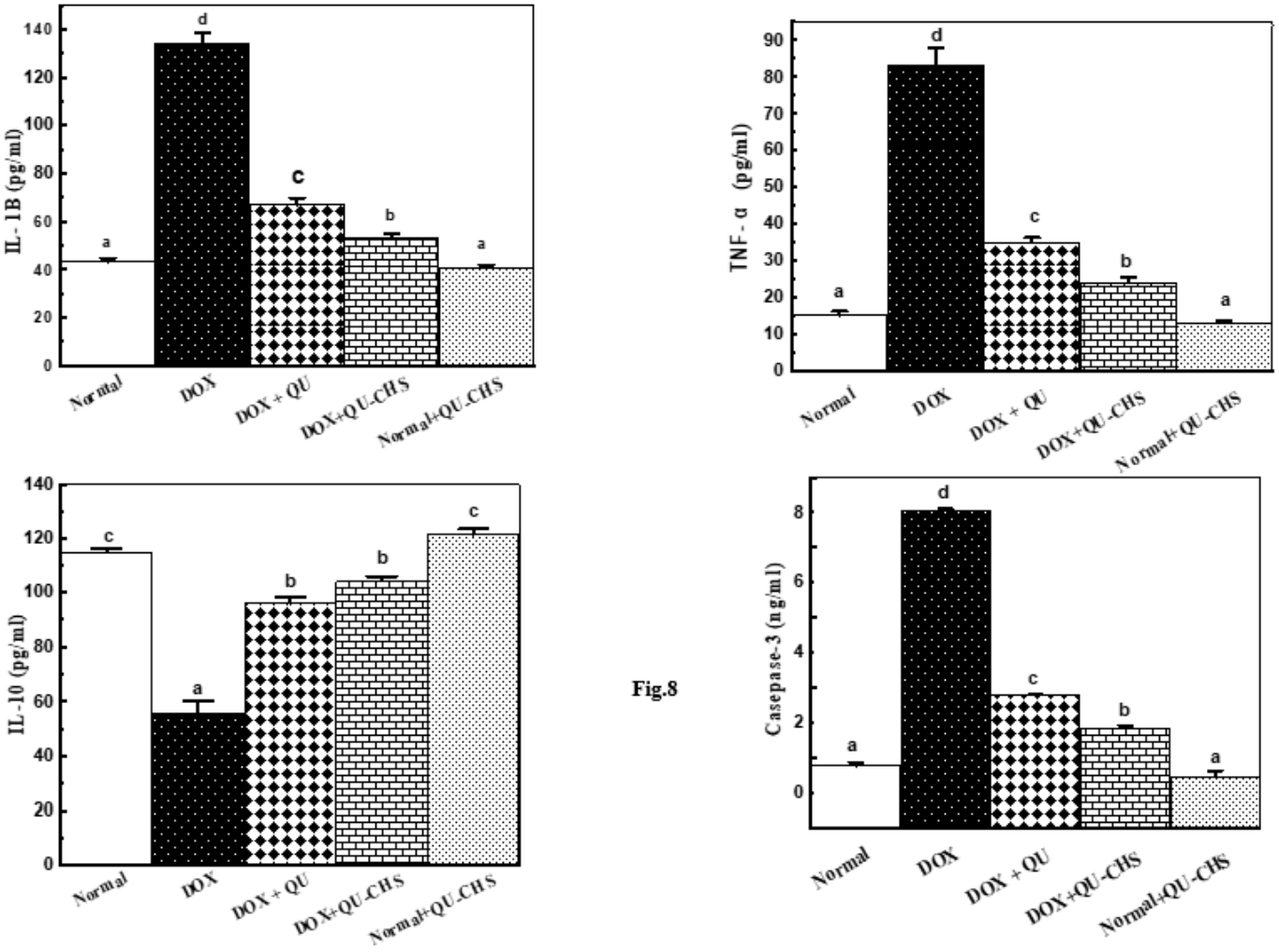

Fig.8

Figure 8

Effect of QU and QU-CHSNPs on serum cytokines IL-1B, TNF-α and IL-10 level and serum apoptotic markers of caspase-3 of normal control and doxorubicin-administered rats.Data are expressed as Mean ± SE. Numbers of samples in each group is six. F-probability: P<0.001 .Values, which share the same superscript symbol, are not significantly different. Interleukin (IL), TNF α Tumor necrosis factor-alpha, DOX (Doxorubicin), QU (Quercetin), QU-CHS (QU-loaded CHSNPs)

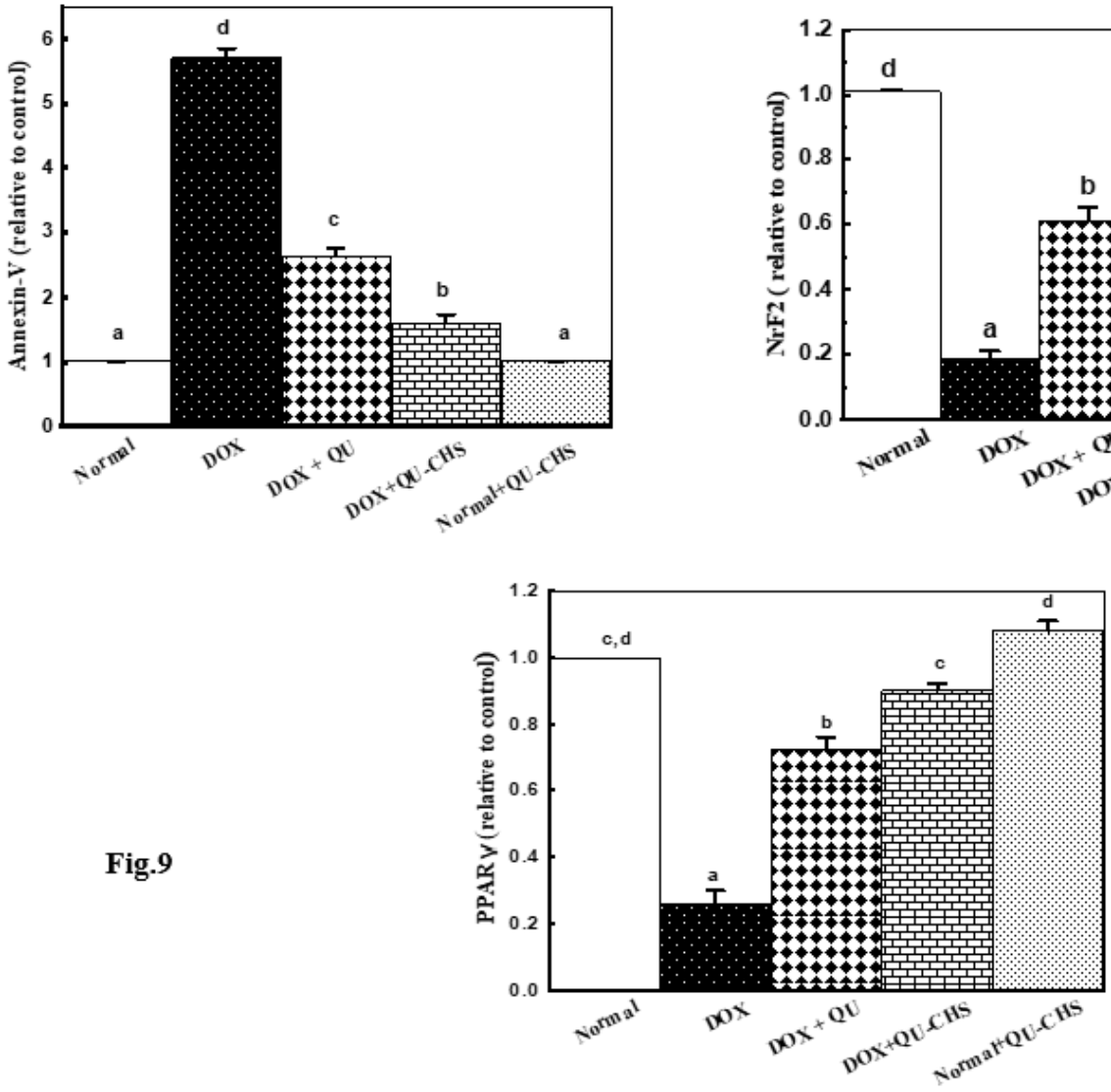

Fig.9

Figure 9

The effect of QU and QU-CHSNPs on cardiac mRNA expression of Annexin-V, NrF2, and PPAR- in normal and doxorubicin-treated rats. The data are presented as mean SE. The number of samples in each group is six. F-probability: P<0.001 values that share the same superscript symbol are not significantly different. NRF2 Nuclear factor erythroid 2-related factor, Peroxisome proliferator-activated receptor gamma 2, DOX (Doxorubicin), QU (Quercetin), QU-CHS (QU-loaded CHSNPs),

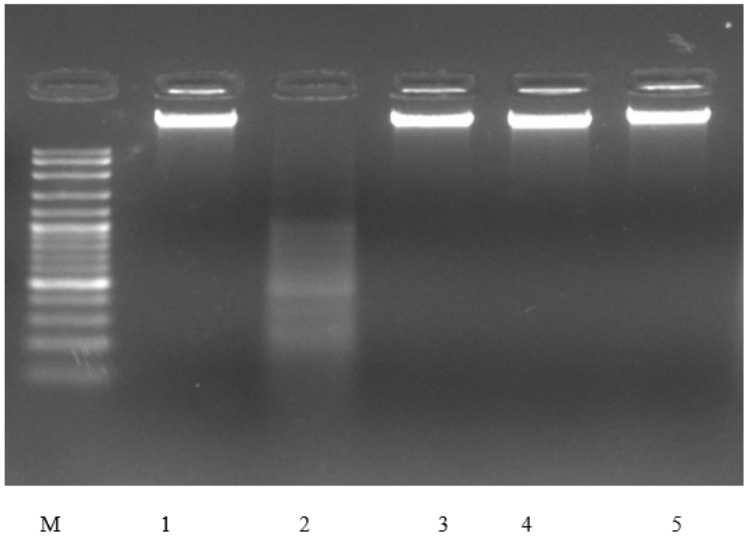

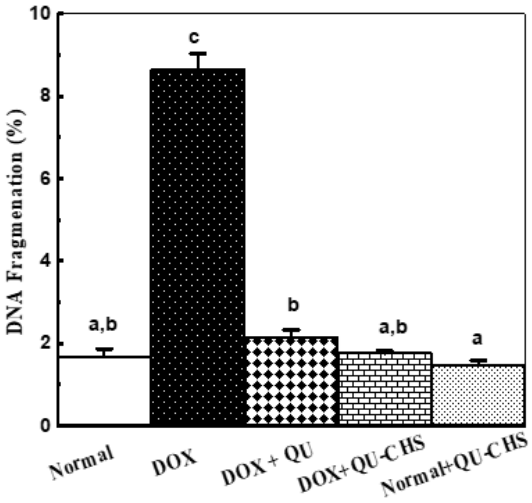

Figure 10

Effect of QU and QU-CHSNPs on Cardiac DNA fragmentation of normal control and DOX-administered Rats. The data are presented as mean SE. The number of samples in each group is six. F-probability: P<0.001 values that share the same superscript symbol are not significantly different. DOX (Doxorubicin), QU (Quercetin), QU-CHS (QU-CHSNPs),

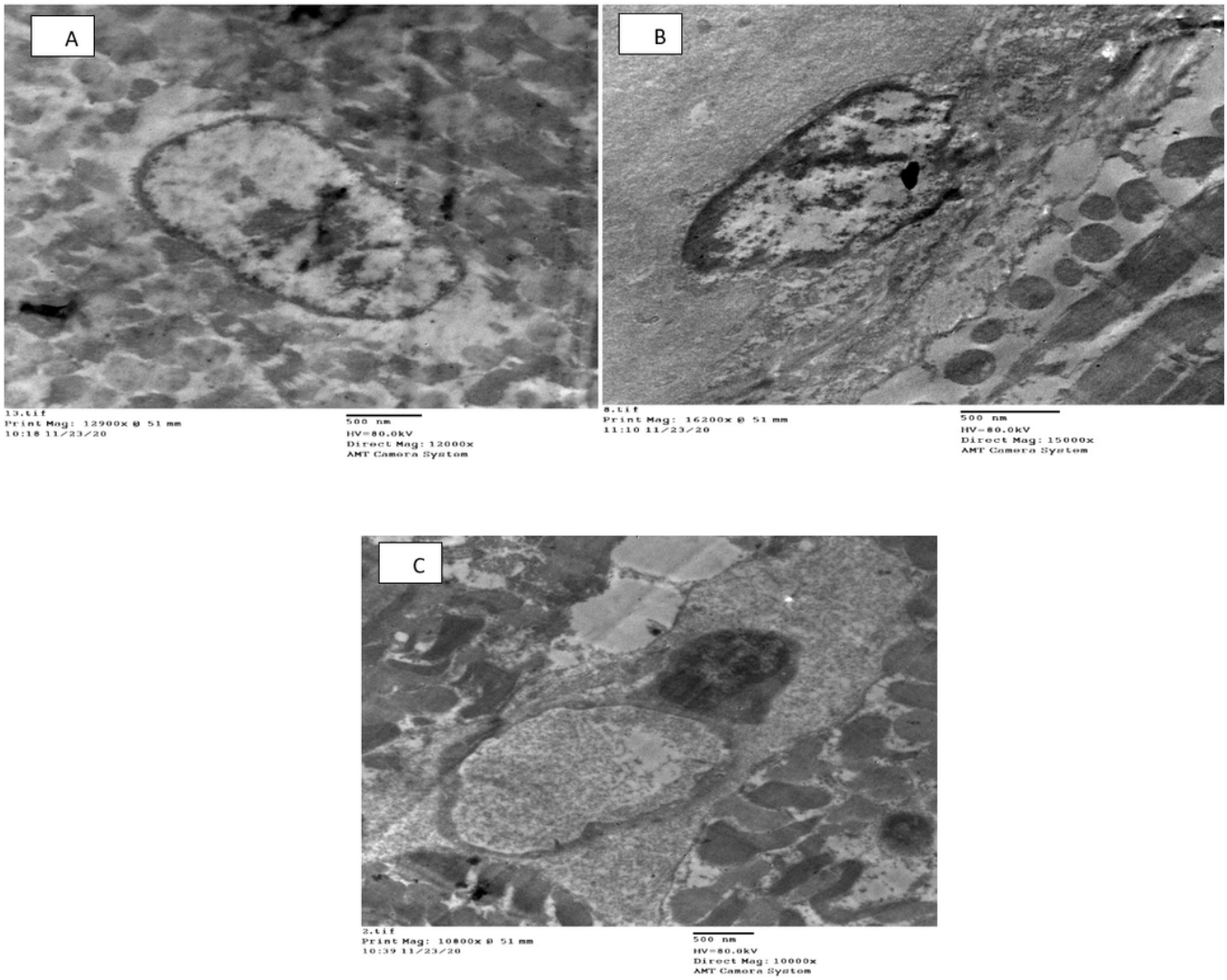

Figure 11

Effect of QU and QU-CHSNPs on Cardiac Electron microscope of normal control and DOX-administered rats

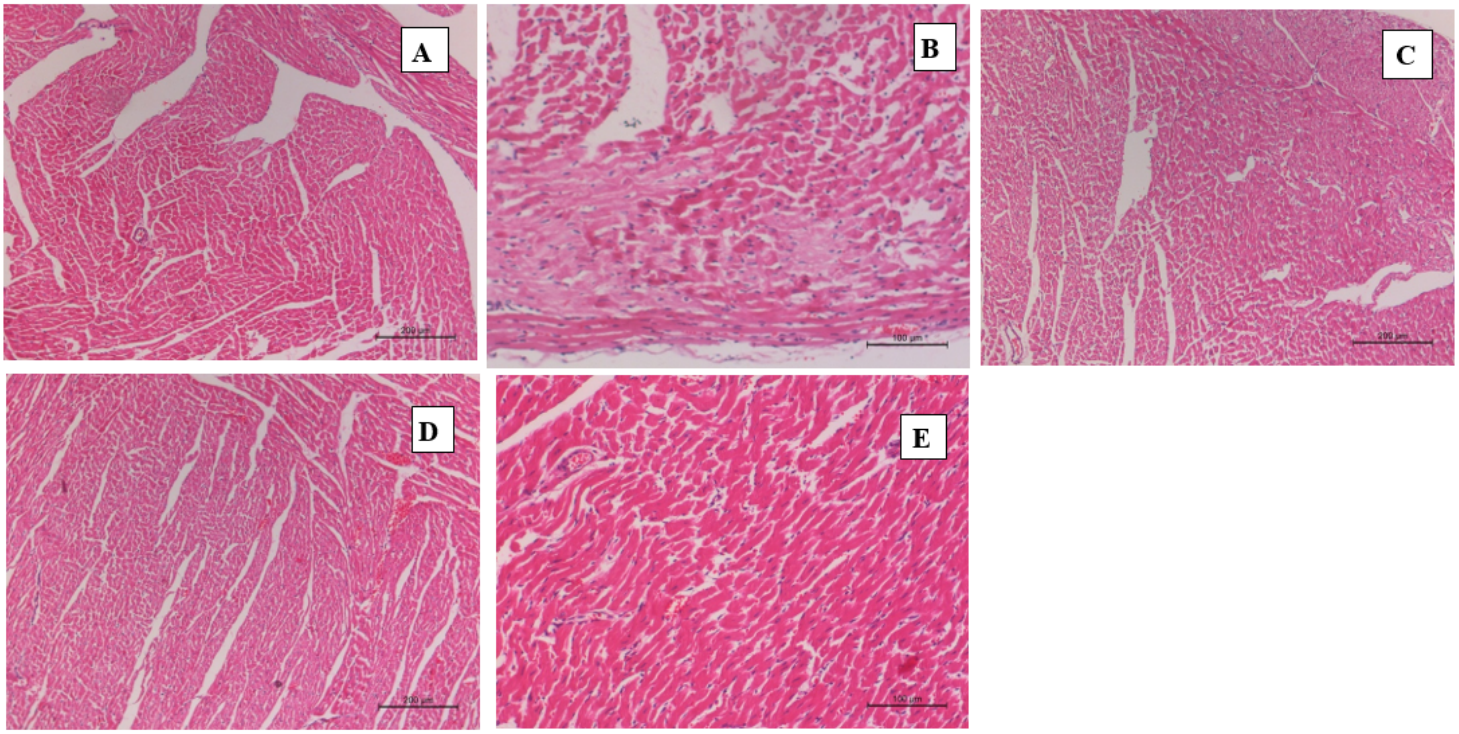

Figure 12

Photomicrographs of H and E stained heart sections of the normal group (10A), DOX-injected group (10B), DOX-injected groups treated with QU (10C), DOX-injected groups treated with QU-CHS (10D), and normal treated with QU-CHSNPs (10E). DOX (Doxorubicin), QU (Quercetin), QU-CHS (QU-CHSNPs